



HAL
open science

A wave-based optimization approach of curved joints for improved defect detection in waveguide assemblies

Vivien Denis, Jean-Mathieu Mencik

► To cite this version:

Vivien Denis, Jean-Mathieu Mencik. A wave-based optimization approach of curved joints for improved defect detection in waveguide assemblies. *Journal of Sound and Vibration*, 2020, 465, pp.115003. 10.1016/j.jsv.2019.115003 . hal-02442812

HAL Id: hal-02442812

<https://hal.science/hal-02442812>

Submitted on 16 Jan 2020

HAL is a multi-disciplinary open access archive for the deposit and dissemination of scientific research documents, whether they are published or not. The documents may come from teaching and research institutions in France or abroad, or from public or private research centers.

L'archive ouverte pluridisciplinaire **HAL**, est destinée au dépôt et à la diffusion de documents scientifiques de niveau recherche, publiés ou non, émanant des établissements d'enseignement et de recherche français ou étrangers, des laboratoires publics ou privés.

A wave-based optimization approach of curved joints for improved defect detection in waveguide assemblies

Vivien Denis, Jean-Mathieu Mencik

INSA Centre Val de Loire, Université d'Orléans, Université de Tours, Laboratoire de Mécanique Gabriel Lamé, 3 Rue de la Chocolaterie, F-41034 Blois, France

Abstract

A wave-based numerical approach is proposed for the detection of defects in waveguide assemblies with curved joints. Within this framework, the wave finite element (WFE) method is used. It provides an efficient numerical means for computing waves in one-dimensional periodic structures (waveguides), and assessing the reflection and transmission coefficients of waves around defects and curved joints. A so-called apparent reflection matrix of the defects, which takes into account the influence of the joints on the reflected signals recorded at some measurement point at the beginning of a waveguide assembly, is proposed. This appears to be the relevant criterion for detecting defects. As it turns out, an optimization procedure for the design of curved joints can be proposed to magnify the amplitude of the reflected signals issued from defects. Numerical experiments are carried out on 2D waveguide assemblies, with one or two curved joints which are parameterized with respect to their radius and angle of curvature. Optimized values of these parameters can be found which magnify the reflected signals issued from several kinds of defects. Time response simulations are finally undertaken

Email address: vivien.denis@insa-cvl.fr (Vivien Denis)

to highlight the relevance of the proposed approach.

Key words: wave finite element method, defect detection, optimization, curved joints, scattering matrix.

1. Introduction

Wave-based non-destructive testing (NDT) techniques are commonly used in mechanical and civil engineering to detect small defects in waveguide structures, e.g., like bridges or pipes. Those defects are mainly due to vibration fatigue or corrosion which affect the integrity of engineering structures. For straight waveguides like beams or pipes, certain waves can travel a long distance and can be well reflected by defects. This is the key idea behind wave-based NDT, i.e., by recording and analyzing the reflected signals (echo) issued from a defect at some measurement point. A common NDT technique hence consists in generating waves (from one or several excitation points), and measuring the reflected waves to determine the occurrence, type and localization of defects [1].

However, engineering structures rarely represent straight infinite waveguides, and mainly involve waveguide assemblies with curved elastic joints. These give rise to local wave reflection/transmission, even wave mode conversion, which can greatly pollute the reflected signals issued from defects (hence impacting their identification). It is therefore crucial to understand the way curved joints can impact the measurement of the reflected waves induced by the defects. This problem has been tackled in various ways in the literature. Demma et al. [2] have analyzed the reflection/transmission coefficients for the waves propagating in two straight waveguides connected to a curved waveguide. Wave mode conversion phenomena among the incident and reflected/transmitted waves in the straight waveguides,

around the curved waveguide, have been investigated. Sanderson et al. [3] have used a finite element (FE) model to estimate the reflection coefficients of waves, from a defect “through” a curved joint; it has been shown that the joint yields an underestimation of the severity of the defect, because of the decrease of the echo
25 amplitude through the joint. To solve this issue, the authors have proposed a strategy to reverse the distortion of the signal induced by the joint to therefore obtain a better characterization of the defect. Verma et al. [4] have analyzed the effect of considering curved joints with different angles and radii of curvature. The authors have highlighted the dependency of the wave transmission coefficients on
30 the curvature angle of the joints, and have reported the effect of constructive and destructive mode interferences. For this task, the authors have considered a time approach and a harmonic excitation. Besides, Ni et al. [5] have investigated the influence of joints of different shapes (Z- or U-shapes) to detect different kinds of defect in pipes. Finally, Sanderson & Catton [6] have proposed a semi analytical
35 FE approach to analyze the way by which multiple defects in pipes interact to each other.

From this literature review, it appears that curved joints are seen in a somewhat negative way, because of their impact on the detection of defects. However, none
40 of these past works have addressed the problem of optimizing the joint properties to improve the sensitivity of the recorded signals to the occurrence of defects. This original challenge has motivated the development of the proposed approach.

It should be also emphasized that the aforementioned works make use of FE models and rely on time approaches to assess the reflection and transmission of
45 waves. The shortcoming of these numerical approaches is that they are computationally cumbersome which is due to the need of a space-time discretization. An

alternative frequency-based, low-cost, numerical approach is developed in this paper. For this purpose, the wave finite element (WFE) method is considered [7, 8]. It provides an efficient numerical means to compute waves in periodic structures, like straight waveguides of arbitrary cross-sections, and compute the reflection and transmission coefficients of these waves at coupling elements like defects or curved joints. Several works have been made within this framework. Mencik and Ichchou [9] have expressed the scattering matrix — i.e., a matrix whose components denote the reflection and transmission coefficients — for waves around coupling elements which can be of arbitrary shapes, and are modeled by means of FE models (see also [10, 11]). Zhou et al. [12] have proposed a time-frequency description of a defect by considering an inverse Fourier transform. Schaal et al. [13] and Bischoff et al. [14] have proposed a hybrid WFE / boundary element method for modeling defect areas in waveguides. Finally, Mencik [11] and Silva et al. [15] have proposed reduced models of joints/junctions by using a component mode synthesis technique. One of the key advantages of the WFE method is that it works in the high frequency range when the waveguides exhibit space-oscillating wave shapes — which are likely to be sensitive to small defects — and when the coupling elements (joints, defects) exhibit local resonance phenomena (component modes).

The present work aims at applying the WFE method to the modeling of waveguide assemblies with curved joints, and which contain a small defect. More precisely, a formulation of the apparent reflection matrix of the defect, which takes into account the influence of the joints on the reflected signals recorded at some measurement point at the beginning of a waveguide assembly, is proposed. From the physical point of view, this work aims at understanding how waves interact

with the defect and the curved joints. A key issue concerns the way the joint properties can be optimized to magnify the amplitudes of the reflected signaled induced by the defect. From the knowledge of the authors, this topic has never
75 been investigated so far.

The rest of the paper is organized as follows. In Sec. 2, the FE model of a waveguide assembly with curved joints, and which contains a defect, is proposed. In Sec. 3, the basics of the WFE method for computing waves in periodic structures are recalled. In Sec. 4, the scattering matrices of the joints and of the defect
80 are expressed; also, the apparent reflection matrix of the defect is formulated. In Sec. 5, the optimization strategy used to magnify the amplitudes of the reflected signals issued from the defect is presented. In Sec. 6, the strategy used to compute the time response of waveguide assemblies is proposed. Finally, in Sec. 7, numerical experiments are carried out by considering 2D waveguide assemblies,
85 with one or two curved joints which are parametrized with respect to their radius and angle of curvature.

2. Problem description

The problem which is tackled here is that of wave propagation in straight waveguides which are connected to curved elastic joints and which contain one
90 defect as shown in Figure 1. Such a waveguide assembly therefore involves several “healthy” homogeneous waveguides, one or several curved joints, and one “coupling element” — also called “defect” — which refers to the part of a waveguide with a defect.

Within the present framework, it is aimed at assessing the waves which are
95 reflected by the defect and which are measured at some receiving points at the

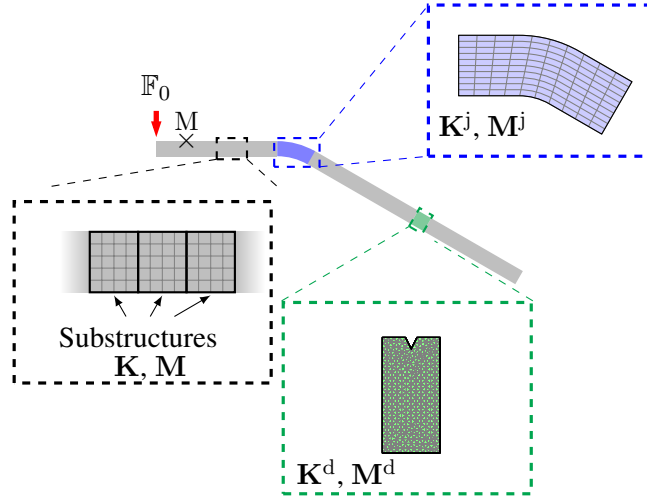


Figure 1: Assembly made up of homogeneous waveguides (gray), a curved joint (blue) and a defect (green). The FE mesh of each homogeneous waveguide is periodic and built from identical substructures; the curved joint and the defect involve full FE meshes. The measurement point is designated by M .

beginning of the structural assembly, i.e., before the joints. 2D/3D FE meshes can be used for modeling the waveguides, the joints as well as the defect. This provides a general means for assessing the wave propagation over broad frequency ranges encompassing the HF range when the waveguide cross-sections exhibit
 100 space-oscillating kinematic fields, and when the dynamics of the joints and of the defect involve many contributing vibration modes.

In the present work, the waveguides are supposed to share the same material properties and the same cross-section. They are modeled by means of periodic FE meshes which are built from identical substructures as shown in Figure 1, and whose FE model is described as follows. Denote as M , C and K the mass, damping and stiffness matrices (respectively) of a substructure expressed in its local reference coordinate system. Hence, in the frequency domain, the dynamic

equilibrium equation of this substructure is expressed as follows:

$$\mathbf{D}\mathbf{q} = \mathbf{F}, \quad (1)$$

where \mathbf{q} and \mathbf{F} refer to the displacement and force vectors, respectively, and \mathbf{D} is the dynamic stiffness matrix (DSM) of the substructure, expressed by:

$$\mathbf{D} = -\omega^2\mathbf{M} + i\omega\mathbf{C} + \mathbf{K}, \quad (2)$$

where ω is the angular frequency, and i is the unit imaginary number.

In the same way, the dynamic equilibrium equations of the defect and of the joints are given by:

$$\mathbf{D}^d\mathbf{q}^d = \mathbf{F}^d, \quad \mathbf{D}^j\mathbf{q}^j = \mathbf{F}^j, \quad (3)$$

where \mathbf{D}^d and \mathbf{D}^j refer to the DSMs of the defect and of the joints, respectively, which are expressed by:

$$\mathbf{D}^d = -\omega^2\mathbf{M}^d + i\omega\mathbf{C}^d + \mathbf{K}^d, \quad \mathbf{D}^j = -\omega^2\mathbf{M}^j + i\omega\mathbf{C}^j + \mathbf{K}^j, \quad (4)$$

where \mathbf{M}^d , \mathbf{C}^d and \mathbf{K}^d (resp. \mathbf{M}^j , \mathbf{C}^j and \mathbf{K}^j) are the mass, damping and stiffness matrices of the defect (resp. the joints). Denote by \mathbf{D}^{d*} and \mathbf{D}^{j*} the condensed DSMs of the defect and of the joints (respectively), i.e., the DSMs once condensed on the interface degrees of freedom (DOFs), i.e., those on the coupling interfaces with the waveguides. The condensed DSMs \mathbf{D}^{d*} and \mathbf{D}^{j*} are given by:

$$\mathbf{D}^{d*} = \mathbf{D}_{\Gamma\Gamma}^d - \mathbf{D}_{\Gamma I}^d(\mathbf{D}_{II}^d)^{-1}\mathbf{D}_{I\Gamma}^d, \quad \mathbf{D}^{j*} = \mathbf{D}_{\Gamma\Gamma}^j - \mathbf{D}_{\Gamma I}^j(\mathbf{D}_{II}^j)^{-1}\mathbf{D}_{I\Gamma}^j, \quad (5)$$

where subscripts Γ and I denote the interface DOFs and internal DOFs (i.e., those which do not belong to the coupling interfaces), respectively. Note that the computation of the condensed DSMs is usually performed by means of the Craig-Bampton (CB) method [11]. In this framework, the displacement vectors for the

internal DOFs are expanded in terms of static modes and a reduced set of fixed interface modes. As a result, the computation of the DSMs can be strongly sped up compared to the classic way when Eq. (5) is considered. Also, the DSM of the substructure is to be condensed on the interface DOFs, which can also be done via the CB method [8].

As for the damping matrices of the substructures, of the defect and of the joints, assumption is made that they are proportional to the mass and stiffness matrices, i.e.:

$$\mathbf{C} = \alpha\mathbf{M} + \beta\mathbf{K} \quad , \quad \mathbf{C}^d = \alpha^d\mathbf{M}^d + \beta^d\mathbf{K}^d \quad , \quad \mathbf{C}^j = \alpha^j\mathbf{M}^j + \beta^j\mathbf{K}^j, \quad (6)$$

where α , β , α^d , β^d , α^j and β^j are positive real numbers.

A whole wave-based matrix equation which models an assembly made up of waveguides, one or several joints and one defect is proposed in the next sections. The strategy involves considering the WFE method for expressing the wave modes which propagate in each waveguide.

3. WFE method

The WFE method aims at analyzing the propagation of waves along one-dimensional periodic structures, i.e., structures whose FE mesh is periodic — i.e., built from identical substructures — along a straight direction as shown in Figure 2.

The WFE method starts by considering the dynamic equilibrium equation of a substructure, which is given by:

$$\mathbf{D}^* \mathbf{q}_\Gamma = \mathbf{F}_\Gamma, \quad (7)$$

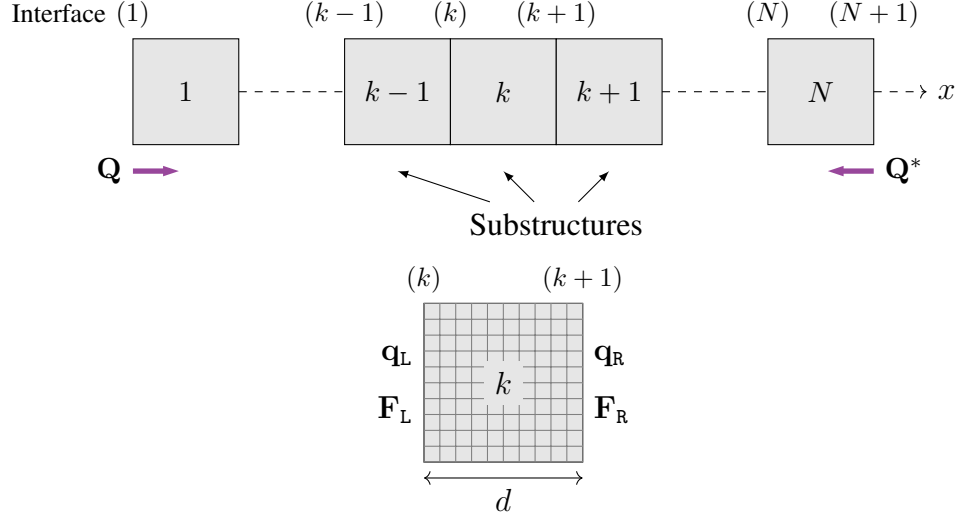


Figure 2: Schematic of a periodic structure.

where \mathbf{D}^* is the condensed DSM of the substructure with respect to the substructure interfaces Γ (see Sec. 2), which are usually referred to as the left (L) and right (R) boundaries (see Figure 2). Note that, due to periodicity conditions, the left and right boundaries of the substructure are meshed in the same way, i.e., with the same number n of DOFs. As a result, Eq. (8) leads to:

$$\begin{bmatrix} \mathbf{D}_{LL}^* & \mathbf{D}_{LR}^* \\ \mathbf{D}_{RL}^* & \mathbf{D}_{RR}^* \end{bmatrix} \begin{bmatrix} \mathbf{q}_L \\ \mathbf{q}_R \end{bmatrix} = \begin{bmatrix} \mathbf{F}_L \\ \mathbf{F}_R \end{bmatrix}, \quad (8)$$

where \mathbf{q}_L and \mathbf{q}_R (resp. \mathbf{F}_L and \mathbf{F}_R) are displacement (resp. force) vectors of size $n \times 1$. Also, \mathbf{D}_{LL}^* , \mathbf{D}_{LR}^* , \mathbf{D}_{RL}^* , \mathbf{D}_{RR}^* are square matrices of size $n \times n$. It is worth pointing out that the mass, damping and stiffness matrices of the substructure are symmetric, which means that the condensed DSM is symmetric and, therefore, that $\mathbf{D}_{LR}^* = (\mathbf{D}_{RL}^*)^T$.

Let us denote by \mathbf{S} the transfer matrix of the substructure, which relates the displacement/force vectors on the right boundary to those on the left boundary as

follows:

$$\begin{bmatrix} \mathbf{q}_R \\ \mathbf{F}_R \end{bmatrix} = \mathbf{S} \begin{bmatrix} \mathbf{q}_L \\ -\mathbf{F}_L \end{bmatrix}. \quad (9)$$

The expression of the transfer matrix \mathbf{S} follows from the dynamic equilibrium equation (8), i.e. (see [9]):

$$\mathbf{S} = \begin{bmatrix} -\mathbf{D}_{LR}^{*-1} \mathbf{D}_{LL}^* & -\mathbf{D}_{LR}^{*-1} \\ \mathbf{D}_{RL}^* - \mathbf{D}_{RR}^* \mathbf{D}_{LR}^{*-1} \mathbf{D}_{LL}^* & -\mathbf{D}_{RR}^* \mathbf{D}_{LR}^{*-1} \end{bmatrix}. \quad (10)$$

Consider now three consecutive substructures $k - 1$, k and $k + 1$ which are separated by two interfaces (k) and $(k + 1)$ as shown in Figure 2. Let us denote by (i) $\mathbf{q}_R^{(k)}$ and $\mathbf{q}_R^{(k+1)}$ the displacement vectors on the right boundaries of the first and second substructures (respectively), (ii) $\mathbf{q}_L^{(k)}$ and $\mathbf{q}_L^{(k+1)}$ the displacement vectors on the left boundaries of the second and third substructures (respectively), (iii) $\mathbf{F}_R^{(k)}$ and $\mathbf{F}_R^{(k+1)}$ the force vectors on the right boundaries of the first and second substructures (respectively), and (iv) $\mathbf{F}_L^{(k)}$ and $\mathbf{F}_L^{(k+1)}$ the force vectors on the left boundaries of the second and third substructures (respectively). In this case, the coupling conditions between the substructures are written as: (i) $\mathbf{q}_R^{(k)} = \mathbf{q}_L^{(k)}$, (ii) $\mathbf{q}_R^{(k+1)} = \mathbf{q}_L^{(k+1)}$, (iii) $\mathbf{F}_R^{(k)} = -\mathbf{F}_L^{(k)}$, and (iv) $\mathbf{F}_R^{(k+1)} = -\mathbf{F}_L^{(k+1)}$. As a result, the transfer matrix relation, Eq. (9), can be rewritten as follows:

$$\begin{bmatrix} \mathbf{q}_R^{(k+1)} \\ \mathbf{F}_R^{(k+1)} \end{bmatrix} = \mathbf{S} \begin{bmatrix} \mathbf{q}_R^{(k)} \\ \mathbf{F}_R^{(k)} \end{bmatrix} \quad \text{or} \quad \begin{bmatrix} \mathbf{q}_L^{(k+1)} \\ -\mathbf{F}_L^{(k+1)} \end{bmatrix} = \mathbf{S} \begin{bmatrix} \mathbf{q}_L^{(k)} \\ -\mathbf{F}_L^{(k)} \end{bmatrix}. \quad (11)$$

Eq. (11) provides a relation to link the displacement and force vectors between two consecutive substructures. It is of the form $\mathbf{u}^{(k+1)} = \mathbf{S}\mathbf{u}^{(k)}$ where the matrix \mathbf{S} is d -periodic (d being the substructure length). According to Bloch's theorem, the eigensolutions of \mathbf{S} represent waves which propagate along the waveguide, i.e.,

the periodic structure resulting from a one-dimensional periodic array of identical substructures, as previously explained. The eigenvalues and eigenvectors of the transfer matrix \mathbf{S} are referred to as the wave modes of the periodic structure. The eigenvalues are denoted by μ_j and are referred to as the wave parameters, with the property that $\mu_j = \exp(-i\beta_j d)$ where β_j stands for the wave numbers. Also, the eigenvectors are denoted by ϕ_j and are referred to as the wave shapes, which are usually partitioned into displacement and force components as follows: $\phi_j = [\phi_{\text{qj}}^T \ \phi_{\text{Fj}}^T]^T$.

Note that the transfer matrix \mathbf{S} is symplectic [9], which means that the eigenvalues come in pairs, say, n eigenvalues μ_j defined so that $|\mu_j| < 1$ and which denote right-going wave modes, and n eigenvalues μ_j^* defined so that $\mu_j^* = 1/\mu_j$ — i.e., $|\mu_j^*| > 1$ — and which denote left-going wave modes. The wave shapes can be partitioned accordingly into n right-going wave modes ϕ_j and n left-going wave modes ϕ_j^* .

Remark 1. The WFE eigenproblem is expressed by $\mathbf{S}\phi_j = \mu_j\phi_j$ and is subject to numerical ill-conditioning. This is explained because the eigenvectors are partitioned into displacement and force components whose values are usually highly disparate, which means that the matrix of eigenvectors is ill-conditioned. A strategy which circumvents this issue is to consider an alternative generalized eigenproblem based on the $\mathbf{S} + \mathbf{S}^{-1}$ transformation technique [16]. One of the key advantages of this generalized eigenproblem is that it is “symplectic structure preserving”, which particularly means that it preserves the analytical relation $\mu_j^* = 1/\mu_j$ between the right-going and left-going wave modes. Hence, the numerical error made for computing the right-going and left-going wave modes can

be highly reduced.

The set of wave shapes $\{\phi_j\}_{j=1}^n \cup \{\phi_j^*\}_{j=1}^n$ constitutes a basis on which the displacement and force vectors of the waveguide can be expanded. For a given
 160 substructure boundary (k), this writes [8]:

$$\mathbf{q}_L^{(k)} = \mathbf{q}_R^{(k)} = \Phi_q \mathbf{Q}^{(k)} + \Phi_q^* \mathbf{Q}^{*(k)}, \quad (12)$$

$$-\mathbf{F}_L^{(k)} = \mathbf{F}_R^{(k)} = \Phi_F \mathbf{Q}^{(k)} + \Phi_F^* \mathbf{Q}^{*(k)}, \quad (13)$$

where Φ_q , Φ_q^* , Φ_F and Φ_F^* are square $n \times n$ matrices defined by $\Phi_q = [\phi_{q1} \cdots \phi_{qn}]$, $\Phi_q^* = [\phi_{q1}^* \cdots \phi_{qn}^*]$, $\Phi_F = [\phi_{F1} \cdots \phi_{Fn}]$ and $\Phi_F^* = [\phi_{F1}^* \cdots \phi_{Fn}^*]$, which are full rank [17]; also, $\mathbf{Q}^{(k)}$ and $\mathbf{Q}^{*(k)}$ are $n \times 1$ vectors of wave amplitudes.

Consider now a waveguide of finite length, i.e., which is composed of a finite
 165 number N of substructures as shown in Figure 2, and denote as \mathbf{Q} and \mathbf{Q}^* the vectors of wave amplitudes at the left and right ends of this waveguide for the right-going and left-going wave modes, respectively. It can be shown that $\mathbf{Q}^{(k)} = \boldsymbol{\mu}^{k-1} \mathbf{Q}$ and $\mathbf{Q}^{*(k)} = \boldsymbol{\mu}^{N+1-k} \mathbf{Q}^*$ where $\boldsymbol{\mu} = \text{diag}\{\mu_j\}_{j=1}^n$ is the $n \times n$ diagonal matrix of the eigenvalues μ_j for the right-going wave modes [8]. As a result, Eqs.
 170 (12) and (13) can be rewritten as follows:

$$\mathbf{q}_L^{(k)} = \mathbf{q}_R^{(k)} = \Phi_q \boldsymbol{\mu}^{k-1} \mathbf{Q} + \Phi_q^* \boldsymbol{\mu}^{N+1-k} \mathbf{Q}^*, \quad (14)$$

$$-\mathbf{F}_L^{(k)} = \mathbf{F}_R^{(k)} = \Phi_F \boldsymbol{\mu}^{k-1} \mathbf{Q} + \Phi_F^* \boldsymbol{\mu}^{N+1-k} \mathbf{Q}^*. \quad (15)$$

4. Scattering matrices

By considering the wave expansions (14) and (15), the reflection and transmission coefficients of waves around the defect and around the joints can be assessed. The strategy is explained hereafter.

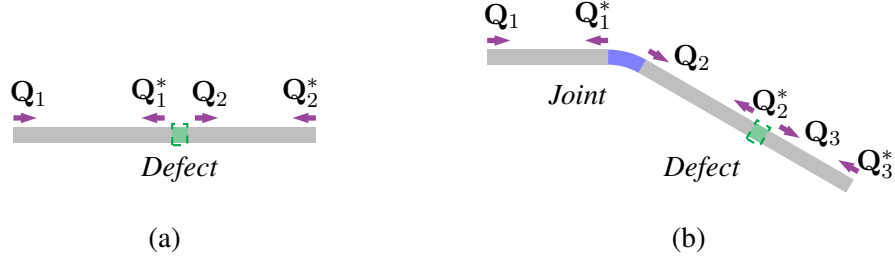


Figure 3: Schematics of one waveguide with a defect (a), and of one waveguide assembly with a curved joint and a defect (b).

Consider first, for the sake of clarity, two waveguides 1 and 2 of similar cross-sections and similar material properties (see Sec. 2), with N_1 and N_2 substructures (respectively), which are connected to a defect — i.e., a waveguide part containing a defect — as shown in Figure 3(a). Denote as Γ_1 the coupling interface between the defect and waveguide 1, and Γ_2 the coupling interface between the defect and waveguide 2. Let us write the dynamic equilibrium equation of the defect as follows:

$$\mathbf{D}^{\text{d}*} \begin{bmatrix} \mathbf{q}^{\text{d}}|_{\Gamma_1} \\ \mathbf{q}^{\text{d}}|_{\Gamma_2} \end{bmatrix} = \begin{bmatrix} \mathbf{F}^{\text{d}}|_{\Gamma_1} \\ \mathbf{F}^{\text{d}}|_{\Gamma_2} \end{bmatrix}, \quad (16)$$

where $\mathbf{D}^{\text{d}*}$ is the condensed DSM of the defect, and $\mathbf{q}^{\text{d}}|_{\Gamma_1}$ and $\mathbf{q}^{\text{d}}|_{\Gamma_2}$ (resp. $\mathbf{F}^{\text{d}}|_{\Gamma_1}$ and $\mathbf{F}^{\text{d}}|_{\Gamma_2}$) are the restrictions of the displacement (resp. force) vector of the defect to Γ_1 and Γ_2 , respectively. Notice that Γ_1 matches the substructure boundary $(N_1 + 1)$ (right side of the first waveguide), while Γ_2 matches the substructure boundary (1) (left side of the second waveguide) (see Sec. 3). As it turns out, the coupling conditions between the defect and the waveguides are expressed as follows:

$$\mathbf{q}^{\text{d}}|_{\Gamma_1} = \mathbf{q}_{\text{R}1}^{(N_1+1)}, \quad \mathbf{q}^{\text{d}}|_{\Gamma_2} = \mathbf{q}_{\text{L}2}^{(1)}, \quad (17)$$

and

$$\mathbf{F}^d|_{\Gamma_1} = -\mathbf{F}_{R1}^{(N_1+1)} \quad , \quad \mathbf{F}^d|_{\Gamma_2} = -\mathbf{F}_{L2}^{(1)} \quad , \quad (18)$$

where subscripts 1 and 2 refer to the displacement and force vectors of waveguides 1 and 2, respectively; also, the minus sign ahead of $\mathbf{F}_{R1}^{(N_1+1)}$ and $\mathbf{F}_{L2}^{(1)}$ results from the action-reaction law. Hence, Eq. (16) yields:

$$\mathbf{D}^{d*} \begin{bmatrix} \mathbf{q}_{R1}^{(N_1+1)} \\ \mathbf{q}_{L2}^{(1)} \end{bmatrix} = - \begin{bmatrix} \mathbf{F}_{R1}^{(N_1+1)} \\ \mathbf{F}_{L2}^{(1)} \end{bmatrix} . \quad (19)$$

175 By expanding $\mathbf{q}_{R1}^{(N_1+1)}$, $\mathbf{q}_{L2}^{(1)}$, $\mathbf{F}_{R1}^{(N_1+1)}$ and $\mathbf{F}_{L2}^{(1)}$ on the basis of wave modes (see Eqs. (14) and (15)), this yields:

$$\mathbf{q}_{R1}^{(N_1+1)} = \Phi_q \mu^{N_1} \mathbf{Q}_1 + \Phi_q^* \mathbf{Q}_1^* , \quad (20)$$

$$\mathbf{q}_{L2}^{(1)} = \Phi_q \mathbf{Q}_2 + \Phi_q^* \mu^{N_2} \mathbf{Q}_2^* , \quad (21)$$

$$\mathbf{F}_{R1}^{(N_1+1)} = \Phi_F \mu^{N_1} \mathbf{Q}_1 + \Phi_F^* \mathbf{Q}_1^* , \quad (22)$$

$$\mathbf{F}_{L2}^{(1)} = - (\Phi_F \mathbf{Q}_2 + \Phi_F^* \mu^{N_2} \mathbf{Q}_2^*) , \quad (23)$$

where \mathbf{Q}_1 and \mathbf{Q}_1^* (resp. \mathbf{Q}_2 and \mathbf{Q}_2^*) are the vectors of wave amplitudes for waveguide 1 (resp. waveguide 2), see Figure 3(a). Introducing Eqs. (20-23) into Eq. (19) leads to:

$$\begin{aligned} \mathbf{D}^{d*} \begin{bmatrix} \Phi_q & \mathbf{0} \\ \mathbf{0} & \Phi_q^* \end{bmatrix} \begin{bmatrix} \mu^{N_1} \mathbf{Q}_1 \\ \mu^{N_2} \mathbf{Q}_2^* \end{bmatrix} + \mathbf{D}^{d*} \begin{bmatrix} \Phi_q^* & \mathbf{0} \\ \mathbf{0} & \Phi_q \end{bmatrix} \begin{bmatrix} \mathbf{Q}_1^* \\ \mathbf{Q}_2 \end{bmatrix} \\ = - \begin{bmatrix} \Phi_F & \mathbf{0} \\ \mathbf{0} & -\Phi_F^* \end{bmatrix} \begin{bmatrix} \mu^{N_1} \mathbf{Q}_1 \\ \mu^{N_2} \mathbf{Q}_2^* \end{bmatrix} - \begin{bmatrix} \Phi_F^* & \mathbf{0} \\ \mathbf{0} & -\Phi_F \end{bmatrix} \begin{bmatrix} \mathbf{Q}_1^* \\ \mathbf{Q}_2 \end{bmatrix} . \end{aligned} \quad (24)$$

180 Eq. (24) gives:

$$\begin{aligned} & \left(\mathbf{D}^{\text{d}*} \begin{bmatrix} \Phi_{\text{q}}^* & \mathbf{0} \\ \mathbf{0} & \Phi_{\text{q}} \end{bmatrix} + \begin{bmatrix} \Phi_{\text{F}}^* & \mathbf{0} \\ \mathbf{0} & -\Phi_{\text{F}} \end{bmatrix} \right) \begin{bmatrix} \mathbf{Q}_1^* \\ \mathbf{Q}_2 \end{bmatrix} \\ &= - \left(\mathbf{D}^{\text{d}*} \begin{bmatrix} \Phi_{\text{q}} & \mathbf{0} \\ \mathbf{0} & \Phi_{\text{q}}^* \end{bmatrix} + \begin{bmatrix} \Phi_{\text{F}} & \mathbf{0} \\ \mathbf{0} & -\Phi_{\text{F}}^* \end{bmatrix} \right) \begin{bmatrix} \mu^{N_1} \mathbf{Q}_1 \\ \mu^{N_2} \mathbf{Q}_2^* \end{bmatrix}, \end{aligned} \quad (25)$$

which can be rewritten as follows:

$$\begin{bmatrix} \mathbf{Q}_1^* \\ \mathbf{Q}_2 \end{bmatrix} = \mathbb{C}^{\text{d}} \begin{bmatrix} \mu^{N_1} \mathbf{Q}_1 \\ \mu^{N_2} \mathbf{Q}_2^* \end{bmatrix} = \begin{bmatrix} \mathbb{C}_{11}^{\text{d}} & \mathbb{C}_{12}^{\text{d}} \\ \mathbb{C}_{21}^{\text{d}} & \mathbb{C}_{22}^{\text{d}} \end{bmatrix} \begin{bmatrix} \mu^{N_1} \mathbf{Q}_1 \\ \mu^{N_2} \mathbf{Q}_2^* \end{bmatrix}, \quad (26)$$

where

$$\mathbb{C}^{\text{d}} = - \left(\mathbf{D}^{\text{d}*} \begin{bmatrix} \Phi_{\text{q}}^* & \mathbf{0} \\ \mathbf{0} & \Phi_{\text{q}} \end{bmatrix} + \begin{bmatrix} \Phi_{\text{F}}^* & \mathbf{0} \\ \mathbf{0} & -\Phi_{\text{F}} \end{bmatrix} \right)^{-1} \left(\mathbf{D}^{\text{d}*} \begin{bmatrix} \Phi_{\text{q}} & \mathbf{0} \\ \mathbf{0} & \Phi_{\text{q}}^* \end{bmatrix} + \begin{bmatrix} \Phi_{\text{F}} & \mathbf{0} \\ \mathbf{0} & -\Phi_{\text{F}}^* \end{bmatrix} \right). \quad (27)$$

Here, \mathbb{C}^{d} is the so-called scattering matrix of the defect. It links the vector of amplitudes $[\mathbf{Q}_1^{*T} \ \mathbf{Q}_2^T]^T$ for the outgoing waves, in waveguides 1 and 2, to the vector of amplitudes $[(\mu^{N_1} \mathbf{Q}_1)^T \ (\mu^{N_2} \mathbf{Q}_2^*)^T]^T$ for the incoming/incident waves. The matrix \mathbb{C}^{d} can be split into block components $\mathbb{C}_{11}^{\text{d}}$, $\mathbb{C}_{12}^{\text{d}}$, $\mathbb{C}_{21}^{\text{d}}$ and $\mathbb{C}_{22}^{\text{d}}$ of size $n \times n$, where (i) $\mathbb{C}_{11}^{\text{d}}$ is the matrix of reflection coefficients for the waves in waveguide 1, (ii) $\mathbb{C}_{22}^{\text{d}}$ is the matrix of reflection coefficients for the waves in waveguide 2, (iii) $\mathbb{C}_{21}^{\text{d}}$ is the matrix of transmission coefficients for the waves in waveguide 1 (to waveguide 2), and (iv) $\mathbb{C}_{12}^{\text{d}}$ is the matrix of transmission coefficients for the waves in waveguide 2 (to waveguide 1).

190

Remark 2. The components of the scattering matrix \mathbb{C}^{d} highly depend on the normalization of the wave shapes ϕ_j and ϕ_j^* , and therefore, on the norms of the

matrices Φ_q , Φ_q^* , Φ_F and Φ_F^* . Hence, it is not guaranteed that the values of the reflection and transmission coefficients are less than one contrary to the academic case when simple bars or beams are dealt with. The issue is mostly linked to the spatial behavior of the wave shapes over the cross-section, which is not uniform and can be oscillating. As a rule of thumb, although not mandatory, it is proposed to normalized the wave shapes w.r.t. their norms, i.e., $\phi_j \rightarrow \phi_j/\|\phi_j\|$ and $\phi_j^* \rightarrow \phi_j^*/\|\phi_j^*\|$.

4.1. Waveguide assembly with one joint

Consider an assembly made up of three healthy waveguides 1, 2 and 3, a joint and a defect as shown in Figure 3(b). The scattering matrix of the joint can be derived in the same way as that of the defect. This yields:

$$\begin{bmatrix} Q_1^* \\ Q_2 \end{bmatrix} = \mathbb{C}^j \begin{bmatrix} \mu^{N_1} Q_1 \\ \mu^{N_2} Q_2^* \end{bmatrix} = \begin{bmatrix} C_{11}^j & C_{12}^j \\ C_{21}^j & C_{22}^j \end{bmatrix} \begin{bmatrix} \mu^{N_1} Q_1 \\ \mu^{N_2} Q_2^* \end{bmatrix}, \quad (28)$$

where \mathbb{C}^j is the scattering matrix of the joint. As for the defect, one has:

$$\begin{bmatrix} Q_2^* \\ Q_3 \end{bmatrix} = \mathbb{C}^d \begin{bmatrix} \mu^{N_2} Q_2 \\ \mu^{N_3} Q_3^* \end{bmatrix} = \begin{bmatrix} C_{22}^d & C_{23}^d \\ C_{32}^d & C_{33}^d \end{bmatrix} \begin{bmatrix} \mu^{N_2} Q_2 \\ \mu^{N_3} Q_3^* \end{bmatrix}, \quad (29)$$

where \mathbb{C}^d is the scattering matrix of the defect. The expressions of the scattering matrices \mathbb{C}^j and \mathbb{C}^d follow from Eq. (27), i.e.:

$$\begin{aligned} \mathbb{C}^j = & - \left(\mathbf{D}^{j*} \begin{bmatrix} \mathcal{L}_1 \Phi_q^* & \mathbf{0} \\ \mathbf{0} & \mathcal{L}_2 \Phi_q \end{bmatrix} + \begin{bmatrix} \mathcal{L}_1 \Phi_F^* & \mathbf{0} \\ \mathbf{0} & -\mathcal{L}_2 \Phi_F \end{bmatrix} \right)^{-1} \\ & \times \left(\mathbf{D}^{j*} \begin{bmatrix} \mathcal{L}_1 \Phi_q & \mathbf{0} \\ \mathbf{0} & \mathcal{L}_2 \Phi_q^* \end{bmatrix} + \begin{bmatrix} \mathcal{L}_1 \Phi_F & \mathbf{0} \\ \mathbf{0} & -\mathcal{L}_2 \Phi_F^* \end{bmatrix} \right), \end{aligned} \quad (30)$$

and

$$\mathbb{C}^d = - \left(\mathbf{D}^{d*} \begin{bmatrix} \mathcal{L}_2 \Phi_q^* & \mathbf{0} \\ \mathbf{0} & \mathcal{L}_3 \Phi_q \end{bmatrix} + \begin{bmatrix} \mathcal{L}_2 \Phi_F^* & \mathbf{0} \\ \mathbf{0} & -\mathcal{L}_3 \Phi_F \end{bmatrix} \right)^{-1} \quad (31)$$

$$\times \left(\mathbf{D}^{d*} \begin{bmatrix} \mathcal{L}_2 \Phi_q & \mathbf{0} \\ \mathbf{0} & \mathcal{L}_3 \Phi_q^* \end{bmatrix} + \begin{bmatrix} \mathcal{L}_2 \Phi_F & \mathbf{0} \\ \mathbf{0} & -\mathcal{L}_3 \Phi_F^* \end{bmatrix} \right),$$

where \mathcal{L}_1 , \mathcal{L}_2 and \mathcal{L}_3 are direction cosine matrices which are introduced here as a means to project the local coordinate systems of waveguides 1, 2 and 3 onto a global reference one [11]. By considering Eqs. (28) and (29), a whole scattering matrix of the system joint - waveguide 2 - defect can be proposed. Indeed, Eqs. (28) and (29) lead to:

$$\begin{bmatrix} \mathbf{Q}_1^* \\ \mathbf{Q}_3 \end{bmatrix} = \begin{bmatrix} \mathbb{C}_{11}^j & \mathbf{0} \\ \mathbf{0} & \mathbb{C}_{33}^d \end{bmatrix} \begin{bmatrix} \mu^{N_1} \mathbf{Q}_1 \\ \mu^{N_3} \mathbf{Q}_3^* \end{bmatrix} + \begin{bmatrix} \mathbb{C}_{12}^j \mu^{N_2} & \mathbf{0} \\ \mathbf{0} & \mathbb{C}_{32}^d \mu^{N_2} \end{bmatrix} \begin{bmatrix} \mathbf{Q}_2^* \\ \mathbf{Q}_2 \end{bmatrix}, \quad (32)$$

and

$$\begin{bmatrix} \mathbf{Q}_2^* \\ \mathbf{Q}_2 \end{bmatrix} = \begin{bmatrix} \mathbf{0} & \mathbb{C}_{23}^d \\ \mathbb{C}_{21}^j & \mathbf{0} \end{bmatrix} \begin{bmatrix} \mu^{N_1} \mathbf{Q}_1 \\ \mu^{N_3} \mathbf{Q}_3^* \end{bmatrix} + \begin{bmatrix} \mathbf{0} & \mathbb{C}_{22}^d \mu^{N_2} \\ \mathbb{C}_{22}^j \mu^{N_2} & \mathbf{0} \end{bmatrix} \begin{bmatrix} \mathbf{Q}_2^* \\ \mathbf{Q}_2 \end{bmatrix}. \quad (33)$$

Eq. (33) yields:

$$\begin{bmatrix} \mathbf{Q}_2^* \\ \mathbf{Q}_2 \end{bmatrix} = \begin{bmatrix} \mathbf{I} & -\mathbb{C}_{22}^d \mu^{N_2} \\ -\mathbb{C}_{22}^j \mu^{N_2} & \mathbf{I} \end{bmatrix}^{-1} \begin{bmatrix} \mathbf{0} & \mathbb{C}_{23}^d \\ \mathbb{C}_{21}^j & \mathbf{0} \end{bmatrix} \begin{bmatrix} \mu^{N_1} \mathbf{Q}_1 \\ \mu^{N_3} \mathbf{Q}_3^* \end{bmatrix}. \quad (34)$$

Therefore, by introducing Eq. (34) into Eq. (32), this gives:

$$\begin{bmatrix} \mathbf{Q}_1^* \\ \mathbf{Q}_3 \end{bmatrix} = \mathbb{C}^{jd} \begin{bmatrix} \mu^{N_1} \mathbf{Q}_1 \\ \mu^{N_3} \mathbf{Q}_3^* \end{bmatrix} = \begin{bmatrix} \mathbb{C}_{11}^{jd} & \mathbb{C}_{13}^{jd} \\ \mathbb{C}_{31}^{jd} & \mathbb{C}_{33}^{jd} \end{bmatrix} \begin{bmatrix} \mu^{N_1} \mathbf{Q}_1 \\ \mu^{N_3} \mathbf{Q}_3^* \end{bmatrix}, \quad (35)$$

where

$$\mathbb{C}^{\text{jd}} = \begin{bmatrix} \mathbb{C}_{11}^{\text{jd}} & \mathbb{C}_{13}^{\text{jd}} \\ \mathbb{C}_{31}^{\text{jd}} & \mathbb{C}_{33}^{\text{jd}} \end{bmatrix} = \begin{bmatrix} \mathbb{C}_{11}^{\text{j}} & \mathbf{0} \\ \mathbf{0} & \mathbb{C}_{33}^{\text{d}} \end{bmatrix} + \begin{bmatrix} \mathbb{C}_{12}^{\text{j}} \boldsymbol{\mu}^{N_2} & \mathbf{0} \\ \mathbf{0} & \mathbb{C}_{32}^{\text{d}} \boldsymbol{\mu}^{N_2} \end{bmatrix} \times \begin{bmatrix} \mathbf{I} & -\mathbb{C}_{22}^{\text{d}} \boldsymbol{\mu}^{N_2} \\ -\mathbb{C}_{22}^{\text{j}} \boldsymbol{\mu}^{N_2} & \mathbf{I} \end{bmatrix}^{-1} \begin{bmatrix} \mathbf{0} & \mathbb{C}_{23}^{\text{d}} \\ \mathbb{C}_{21}^{\text{j}} & \mathbf{0} \end{bmatrix}. \quad (36)$$

The matrix \mathbb{C}^{jd} is to be understood as the scattering matrix of the system joint - waveguide 2 - defect. It links the vector of amplitudes $[\mathbf{Q}_1^{*T} \ \mathbf{Q}_3^T]^T$ for the outgoing waves, in waveguides 1 and 3, to the vector of amplitudes $[(\boldsymbol{\mu}^{N_1} \mathbf{Q}_1)^T \ (\boldsymbol{\mu}^{N_2} \mathbf{Q}_3^*)^T]^T$ for the corresponding incoming/incident waves. More precisely, the block component $\mathbb{C}_{11}^{\text{jd}}$ contains the reflection coefficients for the waves in waveguide 1. It is expressed by

$$\mathbb{C}_{11}^{\text{jd}} = \mathbb{C}_{11}^{\text{j}} + \mathbb{C}_{12}^{\text{j}} \boldsymbol{\mu}^{N_2} \mathbb{C}_{22}^{\text{d}} \boldsymbol{\mu}^{N_2} (\mathbf{I} - \mathbb{C}_{22}^{\text{j}} \boldsymbol{\mu}^{N_2} \mathbb{C}_{22}^{\text{d}} \boldsymbol{\mu}^{N_2})^{-1} \mathbb{C}_{21}^{\text{j}}. \quad (37)$$

To derive Eq. (37), the analytical expression of the inverse of the 2×2 block matrix occurring in Eq. (36) has been invoked. The second matrix on the right hand side of Eq. (37) contains the reflection coefficients of the defect which is seen “through” the joint, i.e., by considering a measurement point located on waveguide 1. Hence, an apparent matrix of reflection coefficients for the defect can be defined as follows:

$$\mathbb{C}_{11}^{\text{d}} = \mathbb{C}_{12}^{\text{j}} \boldsymbol{\mu}^{N_2} \mathbb{C}_{22}^{\text{d}} \boldsymbol{\mu}^{N_2} (\mathbf{I} - \mathbb{C}_{22}^{\text{j}} \boldsymbol{\mu}^{N_2} \mathbb{C}_{22}^{\text{d}} \boldsymbol{\mu}^{N_2})^{-1} \mathbb{C}_{21}^{\text{j}}. \quad (38)$$

205 The underlying issue hence consists in optimizing the joint properties so as to maximize the amplitudes of the waves which are reflected by the defect. In other words, the question which is raised is as whether the joint properties can be tuned in an appropriate way to maximize the components of the matrix $\mathbb{C}_{11}^{\text{d}}$.

4.2. Waveguide assembly with several joints

Let us consider the more general case when $n^j + 1$ waveguides and n^j connecting joints are placed between the measurement point and the defect as shown in Figure 4. In this framework, a joint j_i ($i = 1, \dots, n^j$) connects two consecutive waveguides i and $i + 1$. Denote by N_i and N_{i+1} the numbers of substructures for waveguides i and $i + 1$, respectively. Hence, the scattering matrix of the joint j_i , which links the vectors of wave amplitudes of the outgoing wave modes to those of the incoming ones in waveguides i and $i + 1$, is given by:

$$\begin{bmatrix} \mathbf{Q}_i^* \\ \mathbf{Q}_{i+1} \end{bmatrix} = \mathbb{C}^{j_i} \begin{bmatrix} \boldsymbol{\mu}^{N_i} \mathbf{Q}_i \\ \boldsymbol{\mu}^{N_{i+1}} \mathbf{Q}_{i+1}^* \end{bmatrix} = \begin{bmatrix} \mathbb{C}_{i,i}^{j_i} & \mathbb{C}_{i,i+1}^{j_i} \\ \mathbb{C}_{i+1,i}^{j_i} & \mathbb{C}_{i+1,i+1}^{j_i} \end{bmatrix} \begin{bmatrix} \boldsymbol{\mu}^{N_i} \mathbf{Q}_i \\ \boldsymbol{\mu}^{N_{i+1}} \mathbf{Q}_{i+1}^* \end{bmatrix}. \quad (39)$$

210 where \mathbb{C}^{j_i} is the scattering matrix of the joint j_i , \mathbf{Q}_i^* and \mathbf{Q}_{i+1} are the vectors of wave amplitudes for the outgoing wave modes, and $\boldsymbol{\mu}^{N_i} \mathbf{Q}_i$ and $\boldsymbol{\mu}^{N_{i+1}} \mathbf{Q}_{i+1}^*$ are the vectors of wave amplitudes for the incoming wave modes.

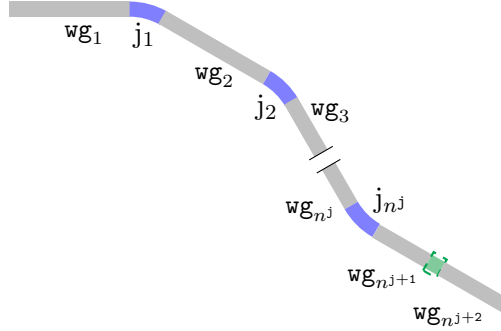


Figure 4: Waveguide assembly involving n^j joints (in blue), $n^j + 2$ waveguides (in gray) and a defect (in green).

The scattering matrix of an assembly involving two joints j_i and j_{i+1} connected through a waveguide $i + 1$ can be expressed by considering the procedure

215 described by Eqs. (32)-(36). This yields:

$$\begin{aligned} \mathbb{C}^{j_i-j_{i+1}} = & \begin{bmatrix} \mathbb{C}_{ii}^{j_i} & \mathbf{0} \\ \mathbf{0} & \mathbb{C}_{i+2,i+2}^{j_{i+1}} \end{bmatrix} + \begin{bmatrix} \mathbb{C}_{i,i+1}^{j_i} \boldsymbol{\mu}^{N_{i+1}} & \mathbf{0} \\ \mathbf{0} & \mathbb{C}_{i+2,i+1}^{j_{i+1}} \boldsymbol{\mu}^{N_{i+1}} \end{bmatrix} \\ & \times \begin{bmatrix} \mathbf{I} & -\mathbb{C}_{i+1,i+1}^{j_{i+1}} \boldsymbol{\mu}^{N_{i+1}} \\ -\mathbb{C}_{i+1,i+1}^{j_i} \boldsymbol{\mu}^{N_{i+1}} & \mathbf{I} \end{bmatrix}^{-1} \begin{bmatrix} \mathbf{0} & \mathbb{C}_{i+1,i+2}^{j_{i+1}} \\ \mathbb{C}_{i+1,i}^{j_i} & \mathbf{0} \end{bmatrix}, \end{aligned} \quad (40)$$

where $\mathbb{C}^{j_i-j_{i+1}}$ is the scattering matrix of the system joint j_i - waveguide $i + 1$ - joint j_{i+1} . Following the same procedure, the formulation of the scattering matrix $\mathbb{C}^{j_i-j_{i+1}}$ can be extended so as to incorporate an additional waveguide $i + 2$ and an additional joint $i + 2$. This yields a new scattering matrix $\mathbb{C}^{j_i-j_{i+2}}$. Hence, an iterative scheme can be proposed to build the global scattering matrix $\mathbb{C}^{j_1-j_{n^j}}$ of an assembly involving n^j joints j_1, j_2, \dots, j_{n^j} and $n^j - 1$ connecting waveguides $2, 3, \dots, n^j$. This yields:

$$\begin{bmatrix} \mathbf{Q}_1^* \\ \mathbf{Q}_{n^j+1} \end{bmatrix} = \mathbb{C}^{j_1-j_{n^j}} \begin{bmatrix} \boldsymbol{\mu}^{N_1} \mathbf{Q}_1 \\ \boldsymbol{\mu}^{N_{n^j+1}} \mathbf{Q}_{n^j+1}^* \end{bmatrix} = \begin{bmatrix} \mathbb{C}_{1,1}^{j_1-j_{n^j}} & \mathbb{C}_{1,n^j+1}^{j_1-j_{n^j}} \\ \mathbb{C}_{n^j+1,1}^{j_1-j_{n^j}} & \mathbb{C}_{n^j+1,n^j+1}^{j_1-j_{n^j}} \end{bmatrix} \begin{bmatrix} \boldsymbol{\mu}^{N_1} \mathbf{Q}_1 \\ \boldsymbol{\mu}^{N_{n^j+1}} \mathbf{Q}_{n^j+1}^* \end{bmatrix}. \quad (41)$$

Assume that the defect is located after the last joint j_{n^j} , i.e., between waveguides $n^j + 1$ and $n^j + 2$ as shown in Figure 4. By considering Eq. (38), the apparent reflection matrix of the defect which is seen in waveguide 1 through the n^j joints turns out to be expressed in this way:

$$\mathbb{C}_{11}^d = \mathbb{C}_{1,n^j+1}^{j_1-j_{n^j}} \boldsymbol{\mu}^{N_{n^j+1}} \mathbb{C}_{n^j+1,n^j+1}^d \boldsymbol{\mu}^{N_{n^j+1}} (\mathbf{I} - \mathbb{C}_{n^j+1,n^j+1}^{j_1-j_{n^j}} \boldsymbol{\mu}^{N_{n^j+1}} \mathbb{C}_{n^j+1,n^j+1}^d \boldsymbol{\mu}^{N_{n^j+1}})^{-1} \mathbb{C}_{n^j+1,1}^{j_1-j_{n^j}}. \quad (42)$$

5. Optimization strategy

Let us denote by $\boldsymbol{\alpha}$ a set of joint parameters such as the internal radius of curvature, the curvature angle, the elastic modulus, and so on. Hence, introduce the following cost function $g(\boldsymbol{\alpha})$:

$$g(\boldsymbol{\alpha}) = \max_{f \in [f_{\min}; f_{\max}]} \|\mathbb{C}_{11}^d(\boldsymbol{\alpha})\|_{\max}, \quad (43)$$

where

$$\|\mathbb{C}_{11}^d(\boldsymbol{\alpha})\|_{\max} = \max_{ij} |(\mathbb{C}_{11}^d)_{ij}(\boldsymbol{\alpha})|. \quad (44)$$

Clearly speaking, $g(\boldsymbol{\alpha})$ represents the maximum value of the max-norm $\|\mathbb{C}_{11}^d(\boldsymbol{\alpha})\|_{\max}$ of the apparent reflection matrix $\mathbb{C}_{11}^d(\boldsymbol{\alpha})$ on a given frequency band $[f_{\min}; f_{\max}]$. In other words, $g(\boldsymbol{\alpha})$ is an upper bound of the absolute values of the components of the matrix $\mathbb{C}_{11}^d(\boldsymbol{\alpha})$ — i.e., $|(\mathbb{C}_{11}^d)_{ij}(\boldsymbol{\alpha})|$ — on $[f_{\min}; f_{\max}]$. The optimization strategy therefore consists in finding the optimal set of parameters $\boldsymbol{\alpha}^{\text{opt}}$ which maximizes this upper bound, i.e.,

$$\boldsymbol{\alpha}^{\text{opt}} = \underset{\boldsymbol{\alpha}}{\operatorname{argmax}} g(\boldsymbol{\alpha}). \quad (45)$$

From the practical point of view, the `fmincon()` or the `particleswarm()` functions of the MATLAB[®] optimization and global optimization toolboxes can be used to solve the optimization problem (45).

220 It should be emphasized that the determination of the cost function $g(\boldsymbol{\alpha})$, for a given set of joint parameters $\boldsymbol{\alpha}$, involves computing the matrix $\mathbb{C}_{11}^d(\boldsymbol{\alpha})$ over a certain frequency band $[f_{\min}; f_{\max}]$, i.e., at several discrete frequencies within $[f_{\min}; f_{\max}]$. The computational burden, if any, is mostly linked to the number of DOFs n which are used to discretize the substructure interfaces (in the waveguides), and the number of internal DOFs which are used to model the joints and

225

the defect. Indeed, a large number of interface DOFs n means an eigenproblem of large size to compute the wave modes, which has to be solved at several discrete frequencies. In practice, computational issues arises as soon as $n > 300$ using MATLAB[®]. The second issue is about the number of internal DOFs of the joints and of the defect which can penalize the computation of the condensed DSMs, see Eq. (5). This is mostly linked to the computation of the matrix inverses $(\mathbf{D}_{\text{II}}^{\text{j}})^{-1}$ and $(\mathbf{D}_{\text{II}}^{\text{d}})^{-1}$, and the computation of the matrix products in Eq. (5). As explained in Sec. 2, this issue can be overcome by considering the CB method where a reduced set of fixed interface modes are used to describe the displacement vector for the internal DOFs. These fixed interface modes can be computed using iterative eigensolvers like the Lanczos method [16]. In this way, the computation of the condensed DSMs can be strongly sped up.

For the sake of clarity, the numerical tasks involved in the computation of the matrix $\mathbb{C}_{11}^{\text{d}}(\alpha)$, at each frequency considered within the frequency band $[f_{\min}; f_{\max}]$, are recalled hereafter:

1. Computation of the condensed DSMs of the joints and of the defect, as well as of the condensed DSM of a substructure (waveguides), Eq. (5).
2. Computation of the wave modes (μ_j, ϕ_j) and (μ_j^*, ϕ_j^*) of the waveguides, see Sec. 3.
3. Computation of the apparent reflection matrix $\mathbb{C}_{11}^{\text{d}}$, Eq. (38) or Eq. (42).

6. Forced response

Recall that the key idea behind the optimization strategy proposed in Sec. 5 is to maximize the reflected signals issued from the defect at some measurement

point located along the first waveguide, i.e., before the joints, when an input time
 250 force is applied to the same waveguide (see Fig.5).

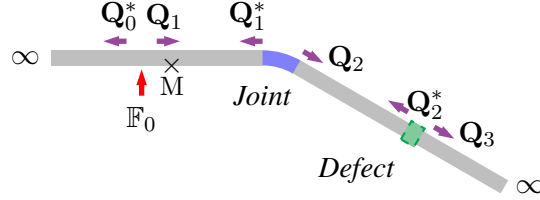


Figure 5: Schematic of an assembly made up of three waveguides, a joint and a defect, which is subject to an input force (first waveguide). The measurement point is designated by M.

Here, assumption is made that the time range analyzed is small enough so that the multiple echos due to the reflections from the left end of the first waveguide and from the right end of the last waveguide are not recorded, which means that those waveguide ends can be considered as infinite boundaries. For the sake of clarity, a schematic of an assembly involving a healthy waveguide subject to one input force, a curved joint, a second healthy waveguide, a defect and a third healthy waveguide, is shown in Fig. 5. Here, the first waveguide is to be split into two waveguides — say, waveguide 0 and waveguide 1 — which are coupled at the location of the input force. Waveguide 2 is located between the joint and the defect, while waveguide 3 is located after the defect. Hence, infinite boundary conditions are to be considered at the left end of waveguide 0, and at the right end of waveguide 3. From the numerical point of view, this is equivalent to canceling out the magnitudes of the outgoing waves, i.e., Q_0 and Q_3^* . As for the coupling conditions between waveguides 0 and 1 at the location of the input force, they are given by:

$$\mathbf{q}_{R0}^{(N_0+1)} = \mathbf{q}_{L1}^{(1)} \quad , \quad \mathbf{F}_{R0}^{(N_0+1)} + \mathbf{F}_{L1}^{(1)} = \mathbf{F} \quad , \quad (46)$$

where \mathbf{F} is the input force vector. By considering the wave expansions (14) and (15) and the fact that $\mathbf{Q}_0 = \mathbf{0}$, this yields:

$$\mathcal{L}_1 \Phi_q^* \mathbf{Q}_0^* = \mathcal{L}_1 \Phi_q \mathbf{Q}_1 + \mathcal{L}_1 \Phi_q^* \boldsymbol{\mu}^{N_1} \mathbf{Q}_1^*, \quad (47)$$

$$\mathcal{L}_1 \Phi_F^* \mathbf{Q}_0^* - \mathcal{L}_1 \Phi_F \mathbf{Q}_1 - \mathcal{L}_1 \Phi_F^* \boldsymbol{\mu}^{N_1} \mathbf{Q}_1^* = \mathcal{L}_1 \mathbf{F}, \quad (48)$$

where N_1 is the number of substructures used to describe waveguide 1, and \mathcal{L}_1 is the direction cosine matrix for both waveguides 1 and 0 (see after Eq. (31)).

255 Notice that the matrix \mathcal{L}_1 is square and invertible, i.e., $(\mathcal{L}_1)^{-1} \mathcal{L}_1 = \mathbf{I}$. As a result, Eqs. (47) and (48) lead to:

$$\mathbf{Q}_0^* - \mathbb{C}_{01}^q \mathbf{Q}_1 - \boldsymbol{\mu}^{N_1} \mathbf{Q}_1^* = \mathbf{0}, \quad (49)$$

$$\mathbf{Q}_1 - \mathbb{C}_{10}^F \mathbf{Q}_0^* - \mathbb{C}_{11}^F \boldsymbol{\mu}^{N_1} \mathbf{Q}_1^* = \mathbb{F}, \quad (50)$$

where $\mathbb{C}_{01}^q = (\Phi_q^*)^{-1} \Phi_q$, $\mathbb{C}_{10}^F = (\Phi_F)^{-1} \Phi_F^*$, $\mathbb{C}_{11}^F = -(\Phi_F)^{-1} \Phi_F^*$ and $\mathbb{F} = -(\Phi_F)^{-1} \mathbf{F}$.

By considering Eqs. (49) and (50) as well as Eqs. (28) and (29), a whole matrix equation can be formulated whose resolution yields the vectors of wave amplitudes for each waveguide (see [18] for further details):

$$\begin{bmatrix} \mathbf{I} & -\mathbb{C}_{11}^F \boldsymbol{\mu}^{N_1} & \mathbf{0} & \mathbf{0} & \mathbf{0} & -\mathbb{C}_{10}^F \\ -\mathbb{C}_{11}^j \boldsymbol{\mu}^{N_1} & \mathbf{I} & \mathbf{0} & -\mathbb{C}_{12}^j \boldsymbol{\mu}^{N_2} & \mathbf{0} & \mathbf{0} \\ -\mathbb{C}_{21}^j \boldsymbol{\mu}^{N_1} & \mathbf{0} & \mathbf{I} & -\mathbb{C}_{22}^j \boldsymbol{\mu}^{N_2} & \mathbf{0} & \mathbf{0} \\ \mathbf{0} & \mathbf{0} & -\mathbb{C}_{22}^d \boldsymbol{\mu}^{N_2} & \mathbf{I} & \mathbf{0} & \mathbf{0} \\ \mathbf{0} & \mathbf{0} & -\mathbb{C}_{32}^d \boldsymbol{\mu}^{N_2} & \mathbf{0} & \mathbf{I} & \mathbf{0} \\ -\mathbb{C}_{01}^q & -\boldsymbol{\mu}^{N_1} & \mathbf{0} & \mathbf{0} & \mathbf{0} & \mathbf{I} \end{bmatrix} \begin{bmatrix} \mathbf{Q}_1 \\ \mathbf{Q}_1^* \\ \mathbf{Q}_2 \\ \mathbf{Q}_2^* \\ \mathbf{Q}_3 \\ \mathbf{Q}_0^* \end{bmatrix} = \begin{bmatrix} \mathbb{F}_0 \\ \mathbf{0} \\ \mathbf{0} \\ \mathbf{0} \\ \mathbf{0} \\ \mathbf{0} \end{bmatrix}. \quad (51)$$

Once the vectors of wave amplitudes \mathbf{Q}_1 , \mathbf{Q}_1^* , \mathbf{Q}_2 , \mathbf{Q}_2^* , \mathbf{Q}_3 and \mathbf{Q}_0^* are computed, the displacement and force vectors of the waveguides can be retrieved by considering the wave expansions (14) and (15), it being understood that $\mathbf{Q}_0 = \mathbf{0}$ and

$\mathbf{Q}_3^* = \mathbf{0}$ (infinite boundary conditions). The interesting feature of the wave-based matrix equation (51) is that its resolution is not expensive from the computational point of view, which is explained because the size of the matrix on the left hand side (Eq. (51)) is small compared to the total number of DOFs that would be used to discretize the whole waveguides. Hence, the displacement vectors can be quickly obtained compared to the conventional resolution techniques like the FE method. In particular, the displacement at the measurement point — namely, q_{mes} —, where the reflected signals are recorded, can be retrieved. Indeed, if one assumes that the measurement point is on waveguide 1, this yields:

$$q_{\text{mes}} = \mathcal{L}_{\text{mes}} \left(\Phi_{\text{q}} \mu^{k_{\text{mes}}-1} \mathbf{Q}_1 + \Phi_{\text{q}}^* \mu^{N_1+1-k_{\text{mes}}} \mathbf{Q}^* \right), \quad (52)$$

where (k_{mes}) denotes the substructure boundary which contains the measurement point, and \mathcal{L}_{mes} is a localization matrix whose purpose is to select the measurement DOF among all the DOFs of the substructure boundary (k_{mes}) .

The aforementioned measured displacement q_{mes} is expressed in the frequency domain. Its expression in the time domain follows from an inverse Fourier transform, i.e.:

$$q_{\text{mes}}(t) = \frac{1}{2\pi} \int_{-\infty}^{+\infty} q_{\text{mes}}(\omega) e^{i\omega t} d\omega. \quad (53)$$

In practice, a discrete inverse Fourier transform is performed [19], which can be done with the `fft()` MATLAB[®] function.

7. Numerical results

The proposed approach is applied to two waveguide assemblies with one and two curved joints, respectively, and which contain a defect as shown in Figure

6. Two kinds of defects are investigated, i.e., (i) a coupling element with a local decrease of the Young's modulus — i.e., $E^d = E(1 - \gamma)$, which represents a crack of dimensions $x^d \times y^d$ (see Figure 6(c)) — referred to as Defect A, and (ii) a coupling element with a triangular notch of width $w^d = 0.01$ m and depth $t^d = 0.01$ m (Figure 6(d)) referred to as Defect B. For each case and each kind of defect, the apparent reflection coefficients of the defect which is seen through the joint(s) at the measurement point (first waveguide) are assessed. Optimization strategies are carried out by following the procedure proposed in Sec. 5. Also, the time response of the first assembly is assessed, and the effect of the variation of the joint parameters on the detection of the defect is highlighted.

The waveguides, the curved joint(s) and the coupling element embedding the defect represent thin elastic structures of height h and cross-section width b , which share the same material properties (see Table 1). The total lengths of waveguides 1, 2 and 3 (see Figure 6) are $l_1 = 2$ m, $l_2 = 0.2$ m and $l_3 = 0.15$ m, respectively. Recall that, within the framework of the WFE method, the waveguides are made of identical substructures. Here, the same substructure, with a length of $d = 2.5 \times 10^{-3}$ m, is used for modeling all the waveguides. As it turns out, 800, 80 and 60 substructures are used to discretize waveguides 1, 2 and 3, respectively.

The substructure, the joint(s) and the defect are meshed with four node plane stress finite elements (with two DOFs per node), except Defect B which is meshed with three nodes triangular elements.

The geometrical properties of the joint(s) and of the defect are listed in Table 2. Each curved joint is parametrized with an internal radius of curvature $R_{\text{int}} \in [0.01; 0.4]$ m and an angle $\theta \in [0; \pi]$ rad. It is surrounded by straight segments of

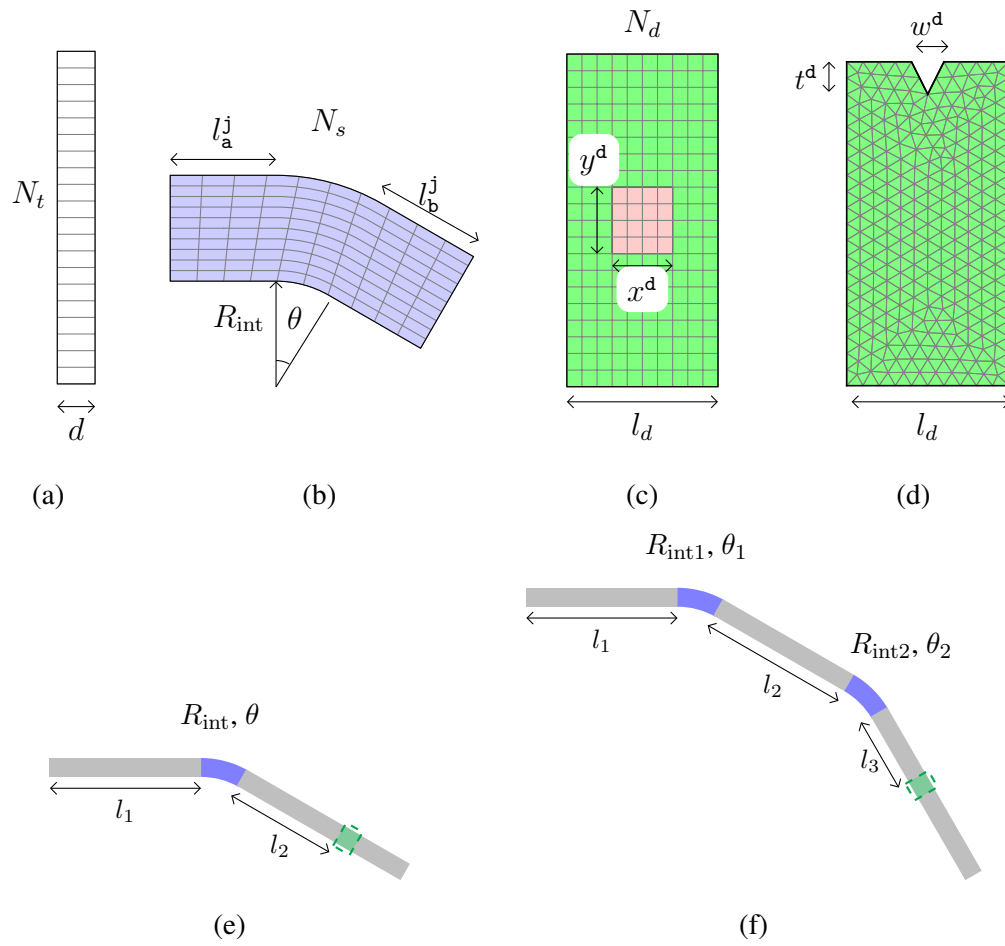


Figure 6: Schematics of a substructure (a), a curved joint (b), a Defect A (local decrease of the Young's modulus) (c), a Defect B (triangular notch) (d), a waveguide assembly with one joint (e) and a waveguide assembly with two joints (f). For the sake of readability, the FE meshes displayed are coarser than those used in the numerical simulations.

small lengths l_a^j and l_b^j as shown in Figure 6(b).¹ Otherwise, when two joints are involved, two radii of curvature $R_{\text{int}1}$ and $R_{\text{int}2}$ and two angles θ_1 and θ_2 are to be considered which can be tuned in an independent way.

305 The substructure which is used to describe the waveguides is meshed with $N_t = 40$ elements along the vertical direction, and does not contain internal DOFs (see Figure 6(a)). This yields $n = 82$ DOFs on the left/right boundaries. Also, $N_s = 160$ elements are used to discretize the joint(s) along the circumferential direction. As for Defect A, $N_d = 20$ elements are used to mesh the longitudinal
310 direction, which yields 800 elements for the whole defect. Also, Defect B is meshed with 3813 triangular elements.

As was pointed out in Sec. 2, the CB method can be used to compute the condensed DSMs of the joint(s) and of the defect, leading to computational saving. Here, a same number of 100 fixed interface modes are used for the joint(s) and the
315 defect, which is supposed to be large enough for obtaining an accurate estimation of the condensed DSMs $\mathbf{D}^{\text{d}*}$ and $\mathbf{D}^{\text{j}*}$ over the frequency band analyzed.

E (GPa)	ρ (kg.m ⁻³)	ν	α (s ⁻¹)	β (s)	h (m)	b (m)
210	7800	0.3	10 ⁻³	10 ⁻⁸	0.1	0.05

Table 1: Material and geometrical properties of the waveguides, of the joint(s) and of the defect (α and β are the damping proportionality coefficients, see Eq. (6)).

¹It is worth pointing out that $\theta = 0$ rad corresponds to the particular case when the curved joint represents a straight waveguide of length $l_a^j + l_b^j$.

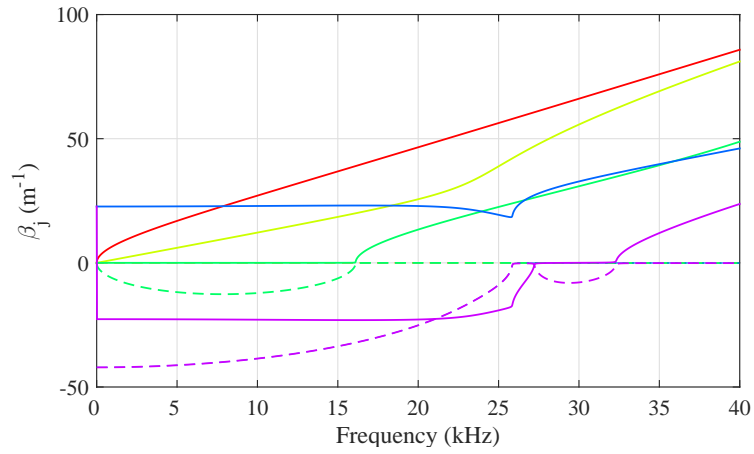
R_{int} (m)	θ (rad)	l_{a}^j (m)	l_{b}^j (m)	l^{d} (m)	x^{d} (m)	y^{d} (m)
[0.01; 0.4]	[0; π]	0.1	0.1	0.05	0.01	0.02

Table 2: Geometrical properties of the joint(s) and of the defect.

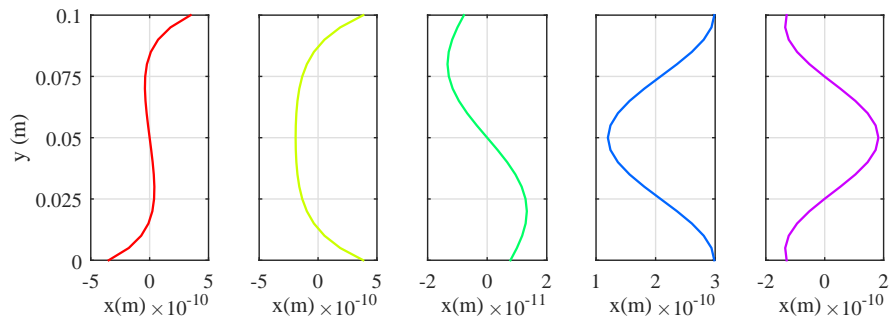
7.1. Reflection coefficients due to the defect

The wave modes of the waveguides are obtained by considering the transfer matrix of a substructure (see Sec. 3). The dispersion curves — i.e., the frequency evolutions of the wave numbers β_j — for five “low order” modes are shown in Figure 7(a) over a frequency range [0; 40] kHz. These modes refer to the flexural wave (in red), the longitudinal wave (in yellow), the shearing wave (in bright green), and two “complex” waves 1 and 2 (in blue and purple). Also, the wave shapes for these modes, at 40 kHz, are displayed in Figure 7(b). It is seen that the wave shapes are not uniform in space, even for the first three basic waves. More precisely, these are $n = 82$ right-going and left-going wave modes which are computed by means of the WFE method, and which are characterized by wave shapes which are not uniform in space and can be highly oscillating. As it turns out, the problem which is tackled here appears to be much more complicated than the simple one consisting in analyzing one-dimensional waveguides like beams, i.e., those for which the cross-section is modeled with one node only.

Let us first consider the case of two waveguides which are straightly connected to a defect, i.e., without joint. The absolute values of the reflection coefficients $(\mathbb{C}_{11}^{\text{d}})_{ij}$ (for $i, j = 1, 2, \dots, 5$) induced by Defect A with a damage severity $\gamma = 0.9$ are shown in Figure 8(a). It is shown that the variation of the reflection coefficients is not monotonic. Instead, several peaks occur for several waves, which means that these waves are locally sensitive — i.e., around 16 kHz and 26



(a)



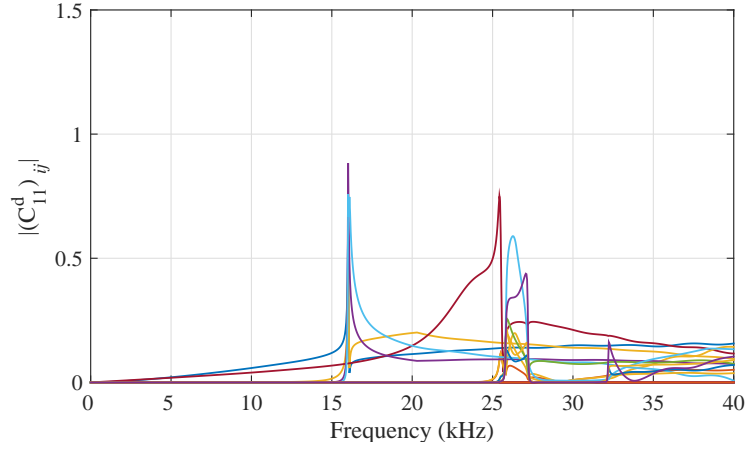
(b)

Figure 7: Real (continuous line) and imaginary (dashed line) parts of the wavenumbers β_j for five “low order” wave modes (a); wave mode shapes at 40 kHz (b).

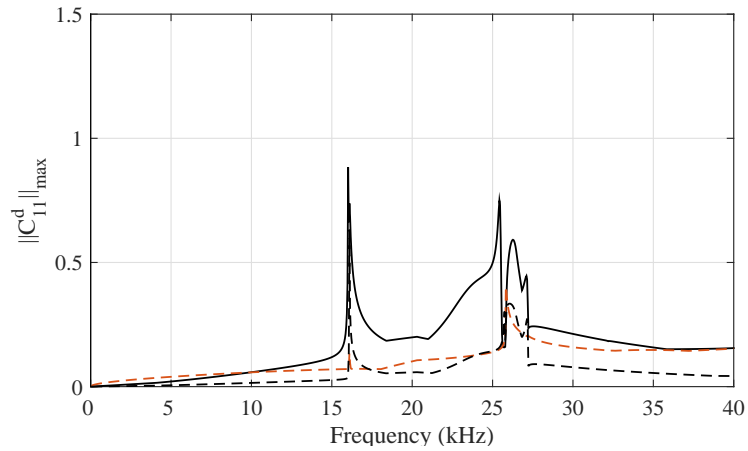
kHz in this case — to the defect. Also, the maximum value of the max-norm of the matrix \mathbb{C}_{11}^d — i.e., $\|\mathbb{C}_{11}^d\|_{\max}$ — is shown in Figure 8(b) for Defect A with $\gamma = 0.9$ and $\gamma = 0.5$, and for Defect B (notch). It is seen that the magnitudes of the reflection coefficients for Defect A with a damage severity of $\gamma = 0.5$ are lower compared to the case where $\gamma = 0.9$ (as expected). However, it remains that the local sensitivities of the reflection coefficients are still well highlighted around 16 kHz and 26 kHz. As for Defect B, waves are becoming sensitive at higher frequencies, say around 26 kHz where the norm $\|\mathbb{C}_{11}^d\|_{\max}$ reaches a local maximum.

7.2. Effects of a curved joint

The absolute values of the components $(\mathbb{C}_{11}^{jd})_{ij}$ (reflection coefficients) of the scattering matrix \mathbb{C}_{11}^{jd} which models the system joint (radius of curvature $R_{\text{int}} = 0.1$) - waveguide - Defect A (severity $\gamma = 0.9$) are displayed in Figure 9(a), see Eq. (38). The frequency evolution of the reflection coefficients appears to be complex compared to the case of a defect without joint, which might be explained because of the energy conversion which occurs between the wave modes through the joint. Also, the max-norms $\|\mathbb{C}_{11}^{jd}\|_{\max}$, $\|\mathbb{C}_{11}^j\|_{\max}$ (effect of the joint only) and $\|\mathbb{C}_{11}^d\|_{\max}$ (effect of the defect through the joint) are plotted in Figures 9(b), 9(c) and 9(d). As it can be seen in Figures 9(c) and 9(d), the energy reflected by the joint is clearly superior to that induced by the defect. Notice however that the defect remains well observable at some local frequencies as shown in Figure 9(d) where the apparent reflection coefficients (components of \mathbb{C}_{11}^d) can exceed 0.5. The effect of the variation of the angle of the joint — i.e., for $\theta = \pi/4$ rad, $\theta = \pi/2$ rad and $\theta = 3\pi/4$ rad — on the apparent reflection coefficients is also highlighted. It is seen that the maximum value of $\|\mathbb{C}_{11}^d\|_{\max}$, e.g., for the peak at



(a)



(b)

Figure 8: Reflection coefficients induced by a defect without joint: reflection coefficients $(\mathbb{C}_{11}^d)_{ij}$ ($i, j = 1, \dots, 5$) for Defect A with $\gamma=0.9$ (a); max-norm $\|\mathbb{C}_{11}^d\|_{\max}$ for Defect A with $\gamma=0.9$ (full black), for Defect A with $\gamma=0.5$ (dashed black) and for Defect B (dashed red) (b).

26 kHz, can largely vary, say with a ratio of 3 between the cases $\theta = \pi/4$ rad and $\theta = 3\pi/4$ rad. It is therefore relevant to propose an adequate design of the joint to magnify the magnitudes of the apparent reflection coefficients.

365

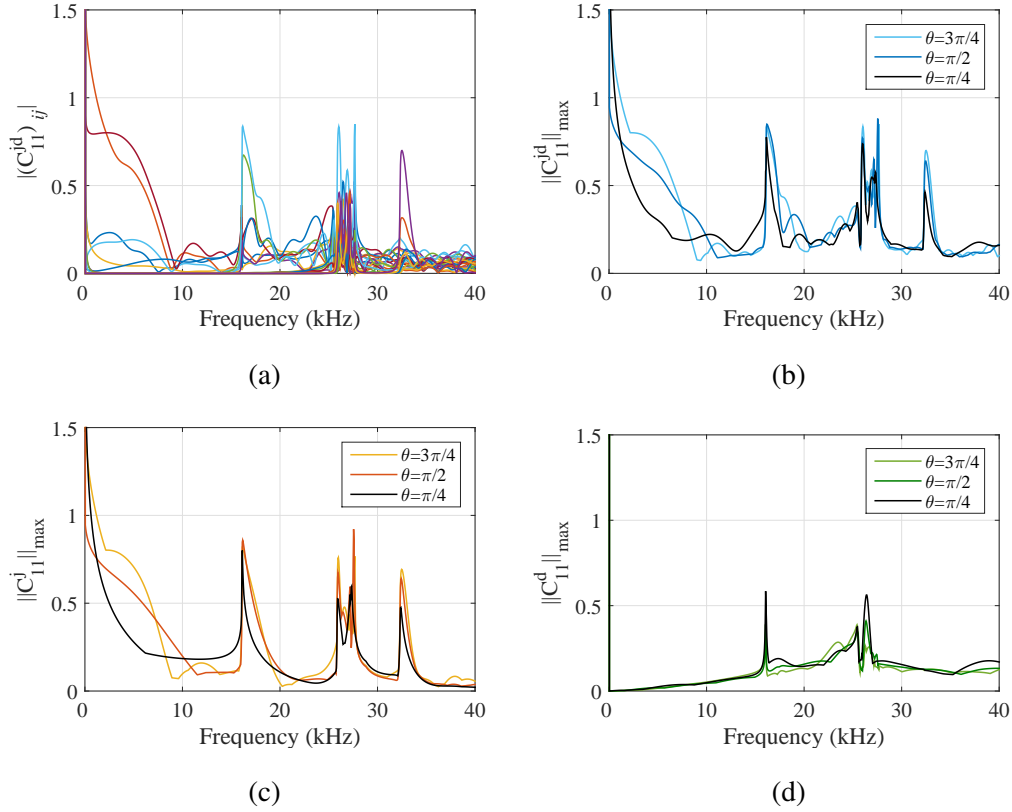


Figure 9: Apparent reflection coefficients (Defect A with $\gamma = 0.9$, and curved joint with $R_{\text{int}} = 0.1$ m): reflection coefficients $(C_{11}^j)^d_{ij}$ for $\theta = 3\pi/4$ rad (a); max-norm $\|C_{11}^j\|_{\max}$ (b); max-norm $\|C_{11}^j\|_{\max}$ (effect of the joint) (c); max-norm $\|C_{11}^d\|_{\max}$ (effect of the defect through the joint) (d).

7.3. Optimization: one curved joint

It is seen in Figures 8(b) and 9(d) that there exist two frequency bands — say, $[15; 17]$ kHz and $[25; 28]$ kHz — on which the apparent reflection coefficients

induced by the defect are high. By considering for instance a Defect A with a
 370 severity $\gamma = 0.9$, a 2D map of the cost function $g(R_{\text{int}}, \theta)$, Eq. (43), can be
 displayed — i.e., when $g(R_{\text{int}}, \theta)$ is plotted against $R_{\text{int}} \in [0.01; 0.4]$ m and $\theta \in$
 $[0; \pi]$ rad — as shown in Figure 10. In particular, Figures 10(a) and 10(c) highlight
 the value of $g(R_{\text{int}}, \theta)$ when $[f_{\text{min}}; f_{\text{max}}] = [15; 17]$ kHz and when $[f_{\text{min}}; f_{\text{max}}] =$
 $[25; 28]$ kHz, respectively. ²

375 Also, the components $(\mathbb{C}_{11}^{\text{d}})_{ij}$ of the reflection matrix $\mathbb{C}_{11}^{\text{d}}$ defined so that
 $|(\mathbb{C}_{11}^{\text{d}})_{ij}| = \|\mathbb{C}_{11}^{\text{d}}\|_{\text{max}}$, i.e., which mostly contribute to the reflected signal in-
 duced by the defect for a given set of parameters (R_{int}, θ) , can be identified, see
 Figures 10(b) and 10(d). For instance, in Figure 10(b), the parameters which yield
 the maximum value of $g(R_{\text{int}}, \theta)$ on $[f_{\text{min}}; f_{\text{max}}] = [15; 17]$ kHz are $R_{\text{int}} = 0.01$
 380 m and $\theta = 0.275$ rad. For this set of parameters, the most contributing com-
 ponent of the reflection matrix is $(\mathbb{C}_{11}^{\text{d}})_{32}$, i.e., the one issued from the coupling
 between the incoming mode 2 and the reflected mode 3. Elsewhere on the do-
 main $[0.01; 0.4]$ m \times $[0; \pi]$ rad, the most contributing components may differ and
 involve different couplings, e.g., between the incoming mode 3 and the reflected
 385 mode 3 (component $(\mathbb{C}_{11}^{\text{d}})_{33}$).

Regarding for instance Figure 10(a) where the maximum of the max-norm
 $\|\mathbb{C}_{11}^{\text{d}}\|_{\text{max}}$ is sought for $f \in [15; 17]$ kHz, it is seen that, for a given value of the
 angle θ (which can be assigned for design purpose), the function $R_{\text{int}} \mapsto g(R_{\text{int}}, \theta)$
 reaches its maximum for a certain value of the internal radius of curvature R_{int}
 390 which does not necessarily matches the minimum and maximum values $R_{\text{int}} =$
 0.01 m and $R_{\text{int}} = 0.4$ m. Results are shown in Figures 11(a) and 11(b) for

²It is worth recalling that $g(R_{\text{int}}, \theta)$ represents the maximum value of the function $f \mapsto$
 $\|\mathbb{C}_{11}^{\text{d}}(R_{\text{int}}, \theta)\|_{\text{max}}$ on $[f_{\text{min}}; f_{\text{max}}]$.

$\theta = \pi/4$ and $\theta = \pi/2$, and for two kinds of defects (Defect A with $\gamma = 0.9$, and Defect B). For each case, it is seen that a “best candidate” R_{int} can be found which does not correspond to the trivial choices $R_{\text{int}} = 0.01$ m and $R_{\text{int}} = 0.4$ m. Figures 395 11(a) and 11(b) highlight results for two different frequency bands, i.e., [15; 17] kHz and [25; 28] kHz respectively. Especially the analysis of $g_{[25;28]\text{kHz}}$ enables one to determine clear maxima for several optimized choices of the internal radius R_{int} , whose determination does not appear to be so straightforward. This gives credit to the proposed optimization approach.

400 7.4. Optimization : two curved joints

Consider two curved joints whose angles is supposed to be tuned to $\theta_1 = \pi/4$ rad and $\theta_2 = -\pi/4$ rad, and whose radii of curvature $R_{\text{int}1}$ and $R_{\text{int}2}$ are supposed to vary independently on $[0.01; 0.4]$ m \times $[0.01; 0.4]$ m. Hence, the aim of the optimization consists in finding the best choices for $R_{\text{int}1}$ and $R_{\text{int}2}$.

405 Figure 12 displays a 2D map of the cost function $g(R_{\text{int}1}, R_{\text{int}2})$ when $[f_{\text{min}}; f_{\text{max}}] = [15; 17]$ kHz for a Defect A (severity $\gamma = 0.9$) located after the second joint. Here again, it is seen that the variation of the cost function is not trivial. By considering the proposed optimization approach, a clear maximum of the cost function can be determined for $R_{\text{int}1} = 0.152$ m and $R_{\text{int}2} = 0.065$ m (see blue dot in 410 Figure 12(a)). Also, the components $(\mathbb{C}_{11}^{\text{d}})_{ij}$ of the reflection matrix $\mathbb{C}_{11}^{\text{d}}$ which mostly contribute to the reflected signal can be identified as shown in Figure 12(b). In the present case, the most contributing component for $R_{\text{int}1} = 0.152$ m and $R_{\text{int}2} = 0.065$ m is $(\mathbb{C}_{11}^{\text{d}})_{22}$, i.e., the one induced by the coupling between the incident mode 2 and the reflected mode 2.

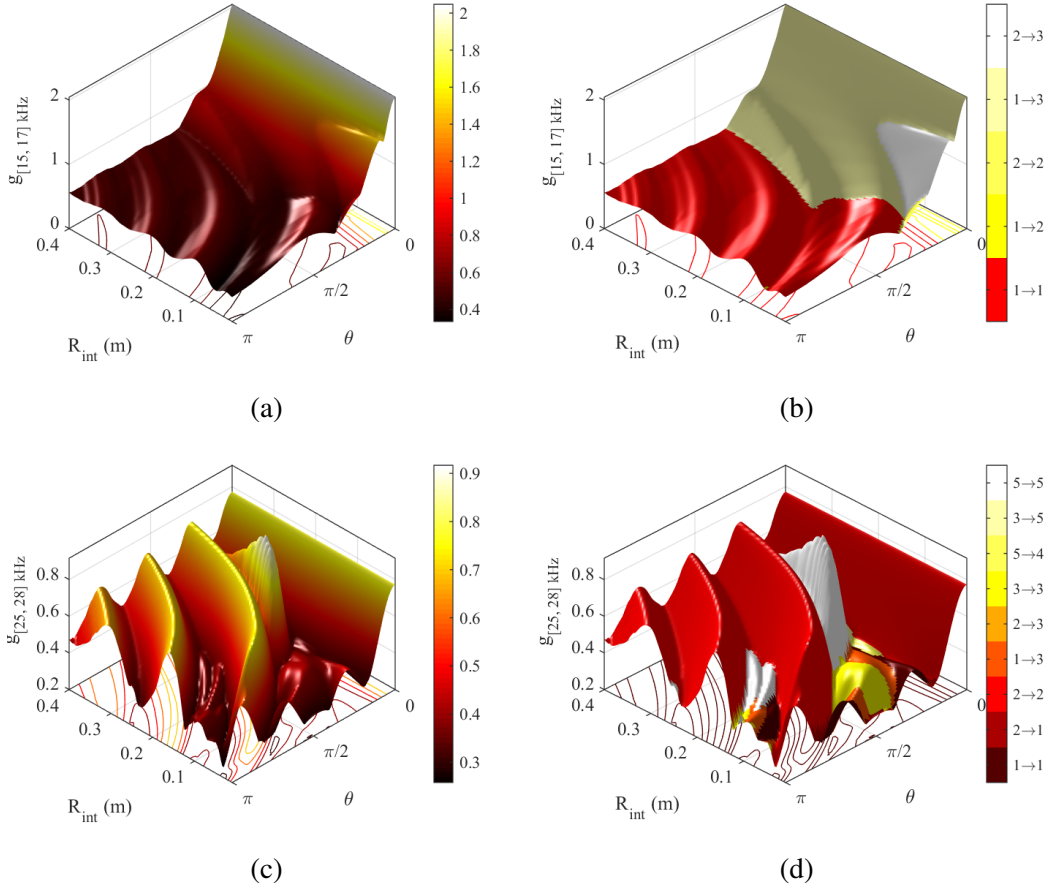
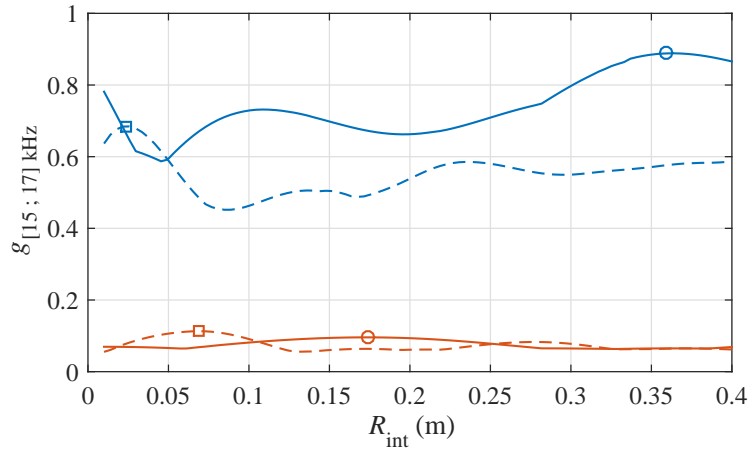
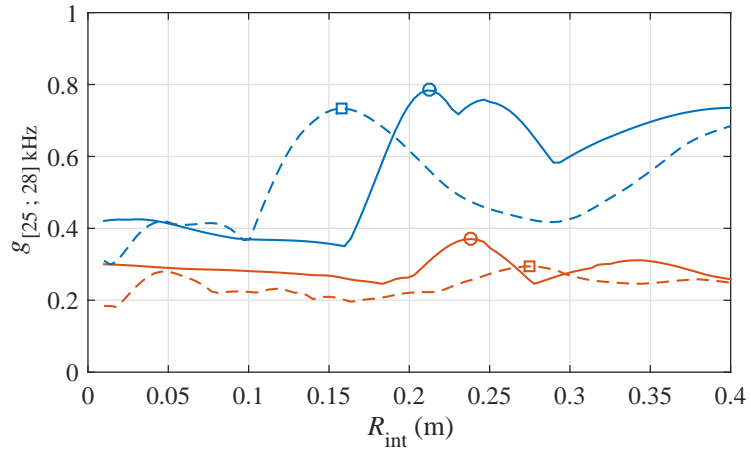


Figure 10: Cost function $g(R_{\text{int}}, \theta)$ for frequency range [15; 17] kHz (a) and corresponding most contributing component $(C_{11}^d)_{ij}$ (b); cost function $g(R_{\text{int}}, \theta)$ for frequency range [25; 28] kHz (c) and corresponding most contributing component $(C_{11}^d)_{ij}$ (d).



(a)



(b)

Figure 11: Variations of the cost functions $g_{[15;17]\text{kHz}}$ (a) and $g_{[25;28]\text{kHz}}$ (b) against R_{int} : Defect A (blue) for $\theta = \pi/4$ rad (full line) and $\theta = \pi/2$ rad (dashed line); Defect B (red) for $\theta = \pi/4$ rad and $\theta = \pi/2$ rad (round and square markers indicate maximum values).

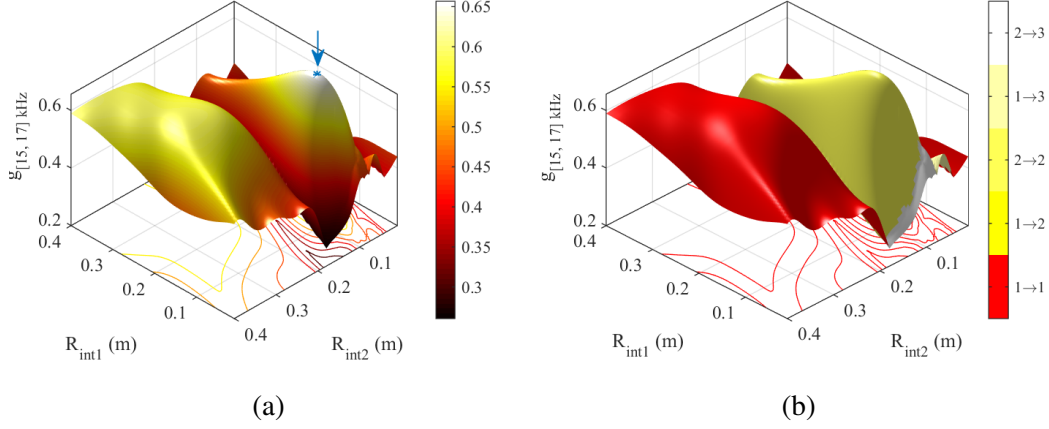


Figure 12: Cost function $g(R_{\text{int}1}, R_{\text{int}2})$ for frequency range $[15; 17]$ kHz and two joints (a) and corresponding most contributing component $(\mathbb{C}_{11}^d)_{ij}$ (b) (blue dot indicates maximal value: $R_{\text{int}1} = 0.152$ m and $R_{\text{int}2} = 0.065$ m).

415 7.5. Time response

To further highlight the results of the previous subsections, the time response at a measurement point located before the joint(s) can be assessed. For the sake of simplicity, a single test case involving one curved joint and a Defect A with a severity $\gamma = 0.9$ is analyzed. Here, the angle of the joint is tuned to $\theta = \pi/2$.
 420 Also, three radii of curvature are considered, i.e., $R_{\text{int}} = 0.1$ m, $R_{\text{int}} = 0.158$ m — which corresponds to the optimized value, see Figure 11(b) — and $R_{\text{int}} = 0.25$ m. The waveguide assembly is excited by a Gaussian pulse at 25.5 kHz along the longitudinal direction, i.e., to excite the longitudinal mode 2 which is supposed to give rise to the most contributing component $(\mathbb{C}_{11}^d)_{22}$ of the reflection matrix
 425 \mathbb{C}_{11}^d (see Sec. 7.3). The measurement point is located 1 m away in front of the excitation point.

Figure 13 displays the incident signal (black curve) along with the reflected

signals for the three test cases ($R_{\text{int}} = 0.1$ m, $R_{\text{int}} = 0.158$ m and $R_{\text{int}} = 0.25$ m). As it can be seen, the case $R_{\text{int}} = 0.158$ m clearly yields the highest reflected signal, which completely agree with what is predicted by the proposed approach (see Sec. 7.3).

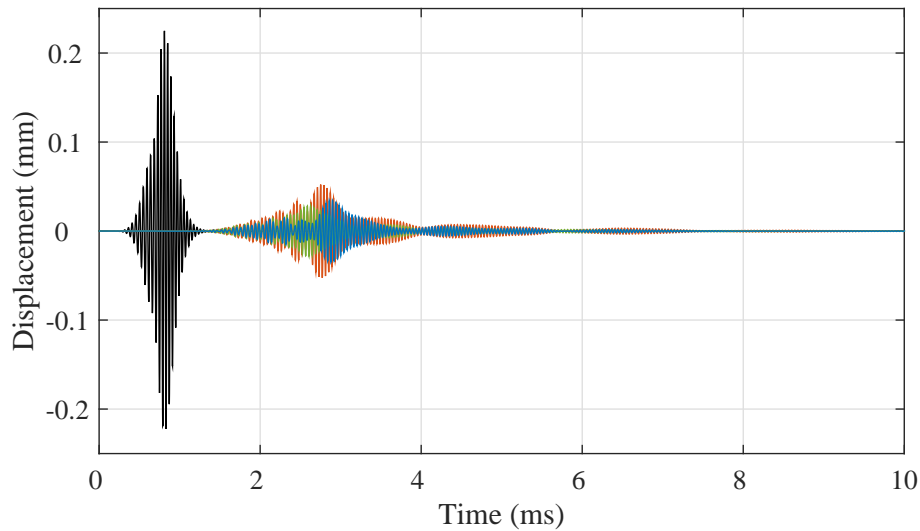


Figure 13: Measured time response for a waveguide assembly involving one curved joint ($\theta = \pi/2$ rad) : incident signal (black); reflected signals for $R_{\text{int}1} = 0.1$ m (green), $R_{\text{int}1} = 0.158$ m (red) and $R_{\text{int}1} = 0.25$ m (blue).

8. Concluding remarks

A wave-based optimization approach has been proposed for detecting defects in waveguide assemblies with curved elastic joints. 2D and 3D FE/WFE models can be used for modeling the waveguides, the joints and the defect parts, which appear to be suitable for predicting space-oscillating wave shapes and local resonance phenomena (cross-section modes and component modes) occurring at high

frequencies, and for describing defects with complex shapes. An original formulation of the apparent reflection matrix of the defects, which takes into account
440 the influence of the joints on the reflected signals recorded at some measurement points at the beginning of a waveguide assembly, has been proposed. This appears to be the relevant criterion for detecting defects. Also, an optimization procedure has been proposed to magnify the reflected signals issued from the defects by tuning the geometrical/material properties of the joints in an appropriate way. The
445 prediction provided by the proposed approach has been validated through time response analysis.

References

- [1] J. L. Rose, A Baseline and Vision of Ultrasonic Guided Wave Inspection Potential, *Journal of Pressure Vessel Technology* 124 (3) (2002) 273. doi:
450 [10.1115/1.1491272](https://doi.org/10.1115/1.1491272).
- [2] A. Demma, P. Cawley, M. Lowe, B. Pavlakovic, The Effect of Bends on the Propagation of Guided Waves in Pipes, *Journal of Pressure Vessel Technology* 127 (2005) 328. doi:[10.1115/1.1990211](https://doi.org/10.1115/1.1990211).
- [3] R. Sanderson, Inspection of pipe networks containing bends using long range
455 guided waves, in: 51st Annual Conference of the British Institute of Non-Destructive Testing 2012, Northamptonshire, United Kingdom, 2012.
- [4] B. Verma, T. K. Mishra, K. Balasubramaniam, P. Rajagopal, Interaction of low-frequency axisymmetric ultrasonic guided waves with bends in pipes of arbitrary bend angle and general bend radius, *Ultrasonics* 54 (3) (2014)
460 801–808. doi:[10.1016/j.ultras.2013.10.007](https://doi.org/10.1016/j.ultras.2013.10.007).
- [5] J. Ni, S. Zhou, P. Zhang, Y. Li, Effect of Pipe Bend Configuration on Guided Waves-Based Defects Detection: An Experimental Study, *Journal of Pressure Vessel Technology* 138 (2015) 021203. doi:[10.1115/1.4031547](https://doi.org/10.1115/1.4031547).
- [6] R. M. Sanderson, P. P. Catton, The Reflection of Guided Waves from Multiple
465 Flaws in Pipes, *Journal of Nondestructive Evaluation* 32 (4) (2013) 384–397. doi:[10.1007/s10921-013-0192-x](https://doi.org/10.1007/s10921-013-0192-x).
- [7] W. X. Zhong, F. W. Williams, On the Direct Solution of Wave Propagation

- for Repetitive Structures, *Journal of Sound and Vibration* 181 (3) (1995) 485–501.
- 470
- [8] J.-M. Mencik, New advances in the forced response computation of periodic structures using the wave finite element (WFE) method, *Computational Mechanics* 54 (3) (2014) 789–801. doi:[10.1007/s00466-014-1033-1](https://doi.org/10.1007/s00466-014-1033-1).
- [9] J.-M. Mencik, M. N. Ichchou, Multi-mode propagation and diffusion in structures through finite elements, *European Journal of Mechanics, A/Solids* 24 (5) (2005) 877–898. doi:[10.1016/j.euromechsol.2005.05.004](https://doi.org/10.1016/j.euromechsol.2005.05.004).
- 475
- [10] M. N. Ichchou, J.-M. Mencik, W. Zhou, Wave finite elements for low and mid-frequency description of coupled structures with damage, *Computer Methods in Applied Mechanics and Engineering* 198 (15-16) (2009) 1311–1326. doi:[10.1016/j.cma.2008.11.024](https://doi.org/10.1016/j.cma.2008.11.024).
- 480
- [11] J.-M. Mencik, Model reduction and perturbation analysis of wave finite element formulations for computing the forced response of coupled elastic systems involving junctions with uncertain eigenfrequencies, *Computer Methods in Applied Mechanics and Engineering* 200 (45-46) (2011) 3051–3065. doi:[10.1016/j.cma.2011.06.014](https://doi.org/10.1016/j.cma.2011.06.014).
- 485
- [12] W. Zhou, M. Ichchou, Wave scattering by local defect in structural waveguide through wave finite element method, *Structural Health Monitoring: An International Journal* 10 (4) (2011) 335–349. doi:[10.1177/14759217110373431](https://doi.org/10.1177/14759217110373431).
- 490

- [13] C. Schaal, S. Bischoff, L. Gaul, Damage detection in multi-wire cables using guided ultrasonic waves, *Structural Health Monitoring: An International Journal* 15 (3) (2016) 279–288. doi:[10.1177/1475921716642747](https://doi.org/10.1177/1475921716642747).
- 495 [14] S. Bischoff, C. Schaal, L. Gaul, Efficient wave scattering analysis for damaged cylindrical waveguides, *Journal of Sound and Vibration* 333 (18) (2014) 4203–4213. doi:[10.1016/j.jsv.2014.04.013](https://doi.org/10.1016/j.jsv.2014.04.013).
- [15] P. B. Silva, J.-M. Mencik, J. R. F. Arruda, Wave finite element-based subelements for forced response analysis of coupled systems via dynamic substructuring, *International Journal for Numerical Methods in Engineering* 500 107 (6) (2015) 453–476. doi:[10.1002/nme](https://doi.org/10.1002/nme).
- [16] J.-M. Mencik, D. Duhamel, A wave-based model reduction technique for the description of the dynamic behavior of periodic structures involving arbitrary-shaped substructures and large-sized finite element models, *Finite Elements in Analysis and Design* 101 (2015) 1–14. doi:[10.1016/j.finel.2015.03.003](https://doi.org/10.1016/j.finel.2015.03.003).
- 505 [17] J.-M. Mencik, On the low- and mid-frequency forced response of elastic structures using wave finite elements with one-dimensional propagation, *Computers & Structures* 88 (11-12) (2010) 674–689. doi:[10.1016/j.compstruc.2010.02.006](https://doi.org/10.1016/j.compstruc.2010.02.006).
- 510 [18] J.-M. Mencik, A wave finite element-based formulation for computing the forced response of structures involving rectangular flat shells, *International Journal for Numerical Methods in Engineering* 95 (2) (2013) 91–120. doi:[10.1002/nme.4494](https://doi.org/10.1002/nme.4494).

- 515 [19] A. Marzani, Time-transient response for ultrasonic guided waves propagating in damped cylinders, *International Journal of Solids and Structures* 45 (25-26) (2008) 6347–6368. doi:[10.1016/j.ijsolstr.2008.07.028](https://doi.org/10.1016/j.ijsolstr.2008.07.028).